

See discussions, stats, and author profiles for this publication at: <https://www.researchgate.net/publication/51532165>

# Lanthanide(III)/Pyrimidine-4,6-dicarboxylate/Oxalate Extended Frameworks: A Detailed Study Based on the Lanthanide Contraction and Temperature Effects

ARTICLE *in* INORGANIC CHEMISTRY · JULY 2011

Impact Factor: 4.76 · DOI: 10.1021/ic201013v · Source: PubMed

---

CITATIONS

36

READS

42

## 9 AUTHORS, INCLUDING:



Javier Cepeda

Universidad del País Vasco / Euskal Herriko ...

33 PUBLICATIONS 280 CITATIONS

[SEE PROFILE](#)



Garikoitz Beobide

Universidad del País Vasco / Euskal Herriko ...

54 PUBLICATIONS 715 CITATIONS

[SEE PROFILE](#)



Oscar Castillo

Universidad del País Vasco / Euskal Herriko ...

133 PUBLICATIONS 1,972 CITATIONS

[SEE PROFILE](#)



Pascual Roman

Universidad del País Vasco / Euskal Herriko ...

192 PUBLICATIONS 3,070 CITATIONS

[SEE PROFILE](#)

# Lanthanide(III)/Pyrimidine-4,6-dicarboxylate/Oxalate Extended Frameworks: A Detailed Study Based on the Lanthanide Contraction and Temperature Effects

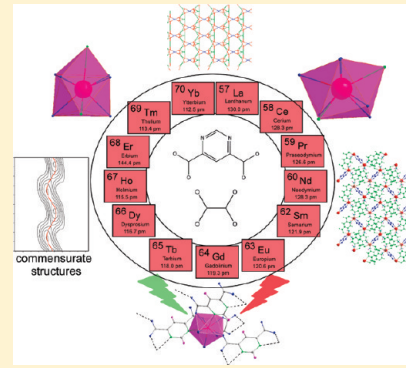
Javier Cepeda,<sup>†</sup> Rolindes Balda,<sup>‡</sup> Garikoitz Beobide,<sup>†</sup> Oscar Castillo,<sup>†,\*</sup> Joaquín Fernández,<sup>‡</sup> Antonio Luque,<sup>†</sup> Sonia Pérez-Yáñez,<sup>†</sup> Pascual Román,<sup>†</sup> and Daniel Vallejo-Sánchez<sup>†</sup>

<sup>†</sup>Departamento de Química Inorgánica, Facultad de Ciencia y Tecnología, Universidad del País Vasco, Apartado 644, E-48080 Bilbao, Spain

<sup>‡</sup>Departamento de Física Aplicada I, Escuela Superior de Ingenieros, Universidad del País Vasco, E-48013 Bilbao, Spain

Supporting Information

**ABSTRACT:** Detailed structural, magnetic, and luminescence studies of six different crystalline phases obtained in the lanthanide/pyrimidine-4,6-dicarboxylate/oxalate system have been afforded:  $\{[\text{Ln}(\mu\text{-pmdc})(\mu\text{-ox})_{0.5}(\text{H}_2\text{O})_2]\cdot3\text{H}_2\text{O}\}_n$  (**1-Ln**),  $\{[\text{Ln}(\mu\text{-pmdc})(\mu\text{-ox})_{0.5}(\text{H}_2\text{O})_3]\cdot2\text{H}_2\text{O}\}_n$  (**2-Ln**),  $\{[\text{Ln}(\mu_3\text{-pmdc})(\mu\text{-ox})_{0.5}(\text{H}_2\text{O})_2]\cdot\sim2.33\text{H}_2\text{O}\}_n$  (**3-Ln**),  $\{[\text{Ln}_2(\mu_3\text{-pmdc})(\mu_4\text{-pmdc})(\mu\text{-ox})(\text{H}_2\text{O})_3]\cdot5\text{H}_2\text{O}\}_n$  (**4-Ln**),  $\{[\text{Ln}(\mu_3\text{-pmdc})(\mu\text{-ox})_{0.5}(\text{H}_2\text{O})_2]\cdot\text{H}_2\text{O}\}_n$  (**5-Ln**), and  $[\text{Ln}(\text{pmdc})_{1.5}(\text{H}_2\text{O})_{2.5}]$  (**6-Ln**). The slow generation of the oxalate (ox) anion, obtained from the in situ partial hydrothermal decomposition of the pyrimidine-4,6-dicarboxylate (pmdc) ligand, allows us to obtain good shaped single crystals, while direct addition of potassium oxalate provides the same compounds but as polycrystalline samples. The crystal structures of all compounds are based on the double chelation established by the pmdc and ox ligands to provide distorted 2D honeycomb layers that, in some cases, are fused together, leading to 3D systems, by replacing some of the coordinated water molecules that complete the coordination sphere of the lanthanide by uncoordinated carboxylate oxygen atoms of the pmdc. The presence of channels occupied by crystallization water molecules is also a common feature with the exception of compounds **5-Ln**. It is worth noting that compounds **3-Ln** present a commensurate crystal structure related to the partial occupancy of the crystallization water molecules placed within the channels. Topological analyses have been carried out, showing a previously nonregistered topology for compounds **4-Ln**, named as **jcr1**. The crystal structures are strongly dependent on the lanthanide ion size and the temperature employed during the hydrothermal synthesis. The lanthanide contraction favors crystal structures involving sterically less hindered coordination environments for the final members of the lanthanide series. Additionally, reinforcement of the entropic effects at high temperatures directs the crystallization process toward less hydrated crystal structures. The magnetic data of these compounds indicate that the exchange coupling between the lanthanide atoms is almost negligible, so the magnetic behavior is dominated by the spin-orbit coupling and the ligand field perturbation. The luminescence properties that exhibit the compounds containing Nd(III), Eu(III), and Tb(III) have been also characterized.



## INTRODUCTION

One of the goals of crystal engineering is to design and synthesize coordination polymers with predetermined topology and properties, usually through judicious selection of multitopic organic ligands as spacers and metal ions or clusters as nodes.<sup>1</sup> As functional metal centers, rare earth metals are attracting more and more attention due to their coordination properties and special chemical characteristics arising from 4f electrons.<sup>2</sup> Many coordination polymers based on rare earths have been synthesized, and most of them exhibit amazing optical and magnetic properties, enabling them as fluorescent probes and electroluminescent devices.<sup>2a,3</sup> However, knowledge about how lanthanide contraction works in crystal-structure formation is limited because of the few systematic investigations across the lanthanide series.<sup>4</sup> It must also be stated that the high coordination number

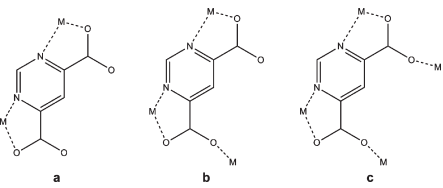
and flexible coordination geometry of rare earth ions make it difficult to predict and control the preparation of rare earth complexes.<sup>5</sup> As it is known, rare earth ions have high affinity for hard donor atoms, so ligands containing oxygen or hybrid oxygen–nitrogen atoms, especially polycarboxylate ligands, are usually employed in the architectures for lanthanide coordination polymers.<sup>4d,6</sup>

With regard to this matter, the pmdc dianion appears to be an appropriate candidate to generate extended lanthanide-based MOFs. In fact, recent use of this dicarboxylate ligand allowed us to achieve the controllable growth of d transition metal complexes of diverse dimensionality.<sup>7</sup> The presence of carboxylate

Received: May 13, 2011

Published: July 29, 2011

**Scheme 1.** Coordination modes of the pmdc ligand in the herein reported complexes: (a)  $\mu\text{-}\kappa N,O:\kappa N',O'\text{-pmdc}$ , (b)  $\mu_3\text{-}\kappa N,O:\kappa N',O':\kappa O''\text{-pmdc}$ , and (c)  $\mu_4\text{-}\kappa N,O:\kappa N',O':\kappa O'':\kappa O'''\text{-pmdc}$



groups in the 4 and 6 positions of the pyrimidinic ring avoids the steric hindrance between the carboxylate groups and confers a planar topology on the dianion. This structural feature favors the bis-chelating mode of the pmdc, but even higher connectivity is also available through its uncoordinated carboxylate oxygen atoms (scheme 1). On the other hand, our experimental work with this ligand under hydrothermal conditions has revealed that its *in situ* partial decomposition generates ox anions in the reaction media. The similarity between the preferred bis-chelating coordination mode of pmdc and ox favors their simultaneous presence as bridging ligands along these compounds.

In this contribution, a wide family of lanthanide/pyrimidine-4,6-dicarboxylate/oxalate-based compounds has been synthesized and structurally and magnetically characterized. Characterization of the luminescence properties of some of these compounds has been also accomplished. The structural diversity has been rationalized based on the Ln(III) size and the temperature employed during the hydrothermal synthesis.

## EXPERIMENTAL PROCEDURES

**Chemicals.** All chemicals were of reagent grade and used as commercially obtained. The starting material pyrimidine-4,6-dicarboxylic acid ( $H_2\text{Pmdc}$ ) was prepared following the previously reported procedure.<sup>8</sup>

**Physical Measurements.** Elemental analyses (C, H, N) were performed on an Euro EA Elemental Analyzer, whereas the metal content, determined by inductively coupled plasma (ICP-AES), was performed on a Horiba Yobin Yvon Activa spectrometer (see Supporting Information). IR spectra (KBr pellets) were recorded on a FTIR 8400S Shimadzu spectrometer in the 4000–400  $\text{cm}^{-1}$  spectral region (see Supporting Information). Magnetic measurements were performed on polycrystalline samples of the complexes with a Quantum Design SQUID susceptometer covering the temperature range 2.0–300 K at a magnetic field of 1000 G. The susceptibility data were corrected for the diamagnetism estimated from Pascal's Tables,<sup>9</sup> the temperature-independent paramagnetism, and the magnetization of the sample holder. Thermal analyses (TG/DTA) were performed on a TA Instruments SDT 2960 thermal analyzer in a synthetic air atmosphere (79%  $N_2$ /21%  $O_2$ ) with a heating rate of 5  $^\circ\text{C}\cdot\text{min}^{-1}$ . The emission measurements were performed at room temperature in a backscattering arrangement using the 488 nm line of an argon laser and a Ti–sapphire ring laser in the 770–920 nm spectral range as the exciting light. The emission from the free sample surface was collected along the backward direction of the incident pump beam with an optical fiber by use of two lenses. Fluorescence was analyzed using a spectrometer (CVI Spectral Products SM-240) in the VIS and a Hamamatsu C9913GC in the near-infrared. Long-pass filters (Semrock LP488 and LP830) were used to remove light at the pump frequency.

**Synthesis of  $\{[\text{Ln}(\mu\text{-pmdc})(\mu\text{-ox})_{0.5}(\text{H}_2\text{O})_2]\cdot 3\text{H}_2\text{O}\}_n$  [Ln = Er (1-Er), Tm (1-Tm), and Yb (1-Yb)]**. A 0.075 mmol amount of  $\text{Tm}(\text{NO}_3)_3\cdot 5\text{H}_2\text{O}$  (0.0334 g) for 1-Tm and  $\text{YbCl}_3\cdot 6\text{H}_2\text{O}$  (0.0291 g) for 1-Yb dissolved in 5 mL of water was added dropwise over a solution of 20 mL containing  $H_2\text{Pmdc}$  (0.0306 g, 0.150 mmol) and kept under vigorous stirring for 1 h at 60 °C. Colorless block-shaped single crystals of 1-Tm and 1-Yb were obtained by placing the resulting solutions on a 45 mL Teflon-lined stainless steel autoclave under autogenous pressure at 140 °C for 3 days and then slowly cooled to room temperature (2 °C/h). Yield: 80–90%. Polycrystalline sample of 1-Er was synthesized following a similar procedure using  $\text{ErCl}_3\cdot 6\text{H}_2\text{O}$  but letting the resulting solution cool faster (10 °C/h).

**Synthesis of  $\{[\text{Ln}(\mu\text{-pmdc})(\mu\text{-ox})_{0.5}(\text{H}_2\text{O})_3]\cdot 2\text{H}_2\text{O}\}_n$  [Ln = Dy (2-Dy) and Er (2-Er)]**. Single crystals were grown following a similar procedure but using  $\text{Dy}(\text{NO}_3)_3$  for 2-Dy,  $\text{ErCl}_3\cdot 6\text{H}_2\text{O}$  for 2-Er, and 120 °C for the hydrothermal treatment. In all cases, the obtained samples contain also single crystals of compounds 3-Ln. The single crystals of 2-Ln suffer a progressive loss of brightness when removing them from the mother liquors, which leads to collapse of the crystal structure.

**Synthesis of  $\{[\text{Ln}(\mu_3\text{-pmdc})(\mu\text{-ox})_{0.5}(\text{H}_2\text{O})_2]\cdot \sim 2.33\text{H}_2\text{O}\}_n$  [Ln = La (3-La), Ce (3-Ce), Pr (3-Pr), Nd (3-Nd), Sm (3-Sm), Eu (3-Eu), Gd (3-Gd), Tb (3-Tb), Dy (3-Dy), Ho (3-Ho), and Er (3-Er)]**. Polycrystalline samples of compounds 3-La, 3-Ce, 3-Pr, and 3-Nd (yield 75–90%) and well-shaped single crystals of compounds 3-Sm, 3-Eu, 3-Gd, 3-Tb, 3-Dy, 3-Ho, and 3-Er (yield 70–85%) were obtained using the above-described general procedure with the temperature for the hydrothermal treatment at 140 °C.

**Synthesis of  $\{[\text{Ln}_2(\mu_3\text{-pmdc})(\mu_4\text{-pmdc})(\mu\text{-ox})(\text{H}_2\text{O})_3]\cdot 5\text{H}_2\text{O}\}_n$  [Ln = La (4-La), Ce (4-Ce), Pr (4-Pr), Nd (4-Nd), Sm (4-Sm), Eu (4-Eu), Gd (4-Gd), Tb (4-Tb), and Dy (4-Dy)]**. Single crystals were grown for compounds 4-La–4-Gd (yield 80–90%), setting the hydrothermal treatment at 140 °C for 4 days. Polycrystalline samples of compounds 4-Tb and 4-Dy were prepared using a hydrothermal temperature of 160 °C; otherwise, they appear as a mixture with compounds 3-Ln.

**Synthesis of  $\{[\text{Ln}(\mu_3\text{-pmdc})(\mu\text{-ox})_{0.5}(\text{H}_2\text{O})_2]\cdot \text{H}_2\text{O}\}_n$  [Ln = La (5-La) and Ce (5-Ce)]**. Prismatic single crystals of 5-La altogether with single crystals of compounds 4-La were grown, setting the hydrothermal temperature at 160 °C. Nevertheless, polycrystalline samples of 5-La and 5-Ce were prepared, cooling the solution directly at room temperature without any controlled cooling ramp.

**Synthesis of  $[\text{Ln}(\text{pmdc})_{1.5}(\text{H}_2\text{O})_{2.5}]$  [Ln = La (6-La), Nd (6-Nd), Tb (6-Tb), Er (6-Er), and Yb (6-Yb)]**. Polycrystalline samples of compounds 6-Tb and 6-Er were obtained employing a hydrothermal temperature at 180 °C. The samples of the remaining 6-Ln compounds show the presence of small amounts of impurities that have been identified as  $\{[\text{Ln}_2(\mu\text{-ox})_3(\text{H}_2\text{O})_6]\cdot 4\text{H}_2\text{O}\}_n$ .<sup>10</sup>

**X-ray Diffraction Data Collection and Structure Determination.** Single crystal diffraction data were collected at 100(2) K on an Oxford Diffraction Xcalibur diffractometer with graphite-monochromated Mo K $\alpha$  radiation ( $\lambda = 0.71073 \text{ \AA}$ ). Data reduction was done with the CrysAlis RED program.<sup>11</sup> Structures of compounds 1-Ln, 2-Ln, 4-Ln, and 5-Ln were solved by direct methods using the SIR92 program<sup>12</sup> and refined by full-matrix least-squares on  $F^2$  including all reflections (SHELXL97).<sup>13</sup> All calculations for these structures were performed using the WINGX crystallographic software package.<sup>14</sup> In the case of compounds 3-Ln, careful examination of the positions of the peaks extracted from the CCD images obtained at 100 K showed that in addition to the main reflections the diffraction pattern also contained strong satellite reflections that could be indexed with four integers as  $\mathbf{H} = ha^* + kb^* + lc^* + mq$  with  $q = (0, 0, 1/3)$ . Therefore, the structures have been considered to be commensurately modulated with an  $a \times b \times 3c$  supercell. Thus, these structures were solved directly in superspace with the charge-flipping algorithm,<sup>15</sup> while the initial structure models were

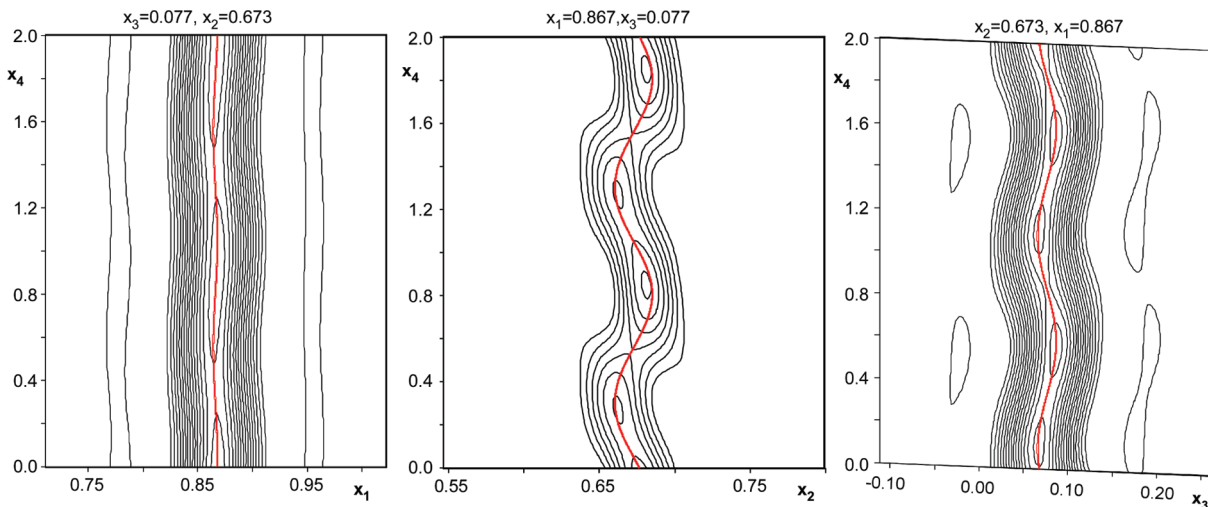


**Figure 1.** Sections through the electron density at the position of the Tb atom in compound 3-Tb: (a)  $x_1-x_4$ , (b)  $x_2-x_4$ , and (c)  $x_3-x_4$  with the representation of the atom once applied the modulation function.

**Table 1. Crystallographic Data and Structure Refinement Details of Compounds 1-Ln and 2-Ln**

|                             | 1-Er                   | 1-Tm                   | 1-Yb                   | 2-Dy                   | 2-Er                   |
|-----------------------------|------------------------|------------------------|------------------------|------------------------|------------------------|
| empirical formula           | $C_7H_{12}ErN_2O_{11}$ | $C_7H_{12}N_2O_{11}Tm$ | $C_7H_{12}N_2O_{11}Yb$ | $C_7H_{12}DyN_2O_{11}$ | $C_7H_{12}ErN_2O_{11}$ |
| fw                          | 467.44                 | 469.11                 | 473.22                 | 462.68                 | 467.44                 |
| cryst syst                  | monoclinic             | monoclinic             | monoclinic             | monoclinic             | monoclinic             |
| space group                 | $C2/c$                 | $C2/c$                 | $C2/c$                 | $P2_1/n$               | $P2_1/n$               |
| $a$ (Å)                     | 18.684(2)              | 18.5717(9)             | 18.589(3)              | 7.8720(6)              | 7.8600(6)              |
| $b$ (Å)                     | 13.079(1)              | 13.0317(3)             | 13.0259(10)            | 13.0190(7)             | 12.9730(8)             |
| $c$ (Å)                     | 14.199(2)              | 13.9718(7)             | 14.065(2)              | 12.9240(8)             | 12.8920(8)             |
| $\beta$ (deg)               | 131.69(4)              | 131.145(8)             | 131.74(2)              | 94.241(6)              | 94.350(6)              |
| $V$ (Å <sup>3</sup> )       | 2591.1(6)              | 2546.4(4)              | 2541.1(6)              | 1320.90(15)            | 1310.78(15)            |
| GOF                         |                        | 0.798                  | 1.024                  | 0.978                  | 1.016                  |
| $R_{\text{int}}$            |                        | 0.0422                 | 0.0289                 | 0.0433                 | 0.0417                 |
| Chi <sup>2</sup>            | 1.65                   |                        |                        |                        |                        |
| final R indices             |                        |                        |                        |                        |                        |
| [ $I > 2\sigma(I)$ ] R1/wR2 |                        | 0.0215/0.0456          | 0.0218/0.0673          | 0.0246/0.0562          | 0.0251/0.0631          |
| all data R1/wR2             |                        | 0.0488/0.0481          | 0.0331/0.0688          | 0.0361/0.0585          | 0.0297/0.0643          |

refined by full-matrix least-squares on  $F$  by using the JANA2006 program,<sup>16</sup> which smoothly converged them to a stable solution. The structure model was further improved by adding harmonic positional modulation waves for all atoms and an occupational modulation to the O5w atom by a crenel function. After averaging the electron density according to the superspace symmetry, we obtained a good estimate of both the basic positions of the atoms and their modulation functions (Figure 1).

Additionally, the anisotropic displacement parameters (ADP) of the metal atoms in compounds 3-Sm, 3-Eu, 3-Gd, and 3-Tb were also found to be modulated. Details of the structure determination and refinement of all compounds are summarized in Tables 1–5. Crystallographic data (excluding structure factors) for the structures reported in this paper have been deposited with the Cambridge Crystallographic Data Center as supplementary publication nos. CCDC 825168–825186. Copies of the data can be obtained free of charge on application to the Director, CCDC, 12 Union Road, Cambridge, CB2 1EZ, U.K. (Fax: +44–1223–335033; e-mail deposit@ccdc.cam.ac.uk or <http://www.ccdc.cam.ac.uk>).

The X-ray powder diffraction (XRPD) patterns were collected on a Phillips X'PERT powder diffractometer with Cu K $\alpha$  radiation ( $\lambda = 1.5418 \text{ \AA}$ ) over the range  $5 < 2\theta < 50^\circ$  with a step size of  $0.02^\circ$  and an

acquisition time of 2.5 s per step at  $25^\circ\text{C}$ . Indexation of the diffraction profiles was made by means of the FULLPROF program (pattern-matching analysis)<sup>17</sup> on the basis of the space group and cell parameters found for isostructural compounds by single-crystal X-ray diffraction. The unit cell parameters obtained in the final refinement are listed in Tables 1–5. The calculated and observed diffraction patterns are shown in the Supporting Information.

Variable-temperature X-ray powder diffraction measurements of compounds 1-Yb, 3-Gd, and 4-Ce were run under ambient atmosphere with heating rates of  $5 \text{ }^\circ\text{C} \cdot \text{min}^{-1}$  and measuring a complete diffractogram every 20 (1-Yb and 3-Gd) or 30  $^\circ\text{C}$  (4-Ce).

## RESULTS AND DISCUSSION

**Structural Description.** X-ray diffraction analyses of all compounds revealed five different crystal structures going from La to Yb and three different coordination modes of the pmde ligand (Scheme 1), presumably as a consequence of the lanthanide contraction and the temperature-reinforced entropic

**Table 2.** Crystallographic Data and Structure Refinement Details of Compounds 3-La–3-Eu

|                     | 3-La  | 3-Ce  | 3-Pr   | 3-Nd  | 3-Sm   | 3-Eu  |
|---------------------|---|---|--|---|--|---|
| empirical formula   | C <sub>7</sub> H <sub>10.66</sub> LaN <sub>2</sub> O <sub>10.33</sub> | C <sub>7</sub> H <sub>10.66</sub> CeN <sub>2</sub> O <sub>10.33</sub> | C <sub>7</sub> H <sub>10.66</sub> N <sub>2</sub> O <sub>10.33</sub> Pr | C <sub>7</sub> H <sub>10.66</sub> NdN <sub>2</sub> O <sub>10.33</sub> | C <sub>7</sub> H <sub>10.66</sub> N <sub>2</sub> O <sub>10.33</sub> Sm | C <sub>7</sub> H <sub>10.66</sub> EuN <sub>2</sub> O <sub>10.33</sub> |
| fw                  | 427.01  | 428.22  | 429.01   | 432.35  | 438.47   | 440.07  |
| cryst syst          | monoclinic  | monoclinic  | monoclinic   | monoclinic  | monoclinic   | monoclinic  |
| superspace group    | P <sub>2</sub> <sub>1</sub> /n(α0γ)0s                                 | P <sub>2</sub> <sub>1</sub> /n(α0γ)0s                                 | P <sub>2</sub> <sub>1</sub> /n(α0γ)0s                                  | P <sub>2</sub> <sub>1</sub> /n(α0γ)0s                                 | P <sub>2</sub> <sub>1</sub> /n(α0γ)0s                                  | P <sub>2</sub> <sub>1</sub> /n(α0γ)0s                                 |
| a (Å)               | 9.665(2)  | 9.694(2)  | 9.693(2)   | 9.736(2)  | 9.7465(3)  | 9.723(1)  |
| b (Å)               | 15.820(4)   | 15.865(3)   | 15.855(3)  | 15.811(5)   | 15.9265(5)   | 15.9092(1)  |
| c (Å)               | 7.871(5)  | 7.921(4)  | 7.915(4)   | 7.941(7)  | 7.9809(7)  | 7.981(2)  |
| β (deg)             | 96.76(5)  | 96.74(1)  | 96.87(1)   | 96.42(1)  | 96.2159(3)   | 96.290(5)   |
| V (Å <sup>3</sup> ) | 1195.0(5)   | 1209.8(4)   | 1207.7(4)  | 1214.67(6)  | 1231.6(2)  | 1227.1(5)   |
| GOF                 |   |   |  |   | 1.71   | 0.98  |
| R <sub>int</sub>    |   |   |  |   | 0.0418   | 0.0425  |
| Chi <sup>2</sup>    | 1.88  | 1.59  | 1.94   | 1.54  |  |   |
| final R indices     |   |   |  |   | 0.0458/0.0576  | 0.0363/0.0382   |
| [I > 3σ(I)] R1/wR2  |   |   |  |   | 0.0728/0.0590  | 0.0795/0.0410   |
| all data R1/wR2     |   |   |  |   |  |   |

**Table 3.** Crystallographic Data and Structure Refinement Details of Compounds 3-Gd–3-Er

|                     | 3-Gd  | 3-Tb   | 3-Dy  | 3-Ho  | 3-Er  |
|---------------------|---|--|---|---|---|
| empirical formula   | C <sub>7</sub> H <sub>10.66</sub> GdN <sub>2</sub> O <sub>10.33</sub> | C <sub>7</sub> H <sub>10.66</sub> N <sub>2</sub> O <sub>10.33</sub> Tb | C <sub>7</sub> H <sub>10.66</sub> DyN <sub>2</sub> O <sub>10.33</sub> | C <sub>7</sub> H <sub>10.66</sub> HoN <sub>2</sub> O <sub>10.33</sub> | C <sub>7</sub> H <sub>10.66</sub> ErN <sub>2</sub> O <sub>10.33</sub> |
| fw                  | 445.36  | 447.03   | 450.61  | 453.04  | 455.37  |
| cryst syst          | monoclinic  | monoclinic   | monoclinic  | monoclinic  | monoclinic  |
| superspace group    | P <sub>2</sub> <sub>1</sub> /n(α0γ)0s                                 | P <sub>2</sub> <sub>1</sub> /n(α0γ)0s                                  | P <sub>2</sub> <sub>1</sub> /n(α0γ)0s                                 | P <sub>2</sub> <sub>1</sub> /n(α0γ)0s                                 | P <sub>2</sub> <sub>1</sub> /n(α0γ)0s                                 |
| a (Å)               | 9.693(1)  | 9.664(4)   | 9.650(4)  | 9.6219(3)   | 9.5926(3)   |
| b (Å)               | 15.869(1)   | 15.844(7)  | 15.845(5)   | 15.8216(4)  | 15.7938(4)  |
| c (Å)               | 7.955(1)  | 7.959(1)   | 7.955(3)  | 7.9375(2)   | 7.9230(3)   |
| β (deg)             | 96.356(6)   | 96.489(4)  | 96.555(4)   | 96.625(3)   | 96.759(3)   |
| V (Å <sup>3</sup> ) | 1216.1(1)   | 1210.9(4)  | 1208.4(1)   | 1200.3(1)   | 1192.02(7)  |
| GOF                 | 1.47  | 1.60   | 2.29  | 1.23  | 3.33  |
| R <sub>int</sub>    | 0.0374  | 0.0367   | 0.0350  | 0.0471  | 0.0302  |
| final R indices     |   |  |   |   |   |
| [I > 3σ(I)] R1/wR2  | 0.0359/0.0417   | 0.0324/0.0389  | 0.0524/0.0606   | 0.0412/0.0428   | 0.0690/0.0772   |
| all data R1/wR2     | 0.0552/0.0430   | 0.0488/0.0404  | 0.0737/0.0623   | 0.0799/0.0457   | 0.0879/0.0790   |

**Table 4.** Crystallographic Data and Structure Refinement Details of Compounds 4-La–4-Sm

|                     | 4-La   | 4-Ce   | 4-Pr   | 4-Nd   | 4-Sm   |
|---------------------|--|--|--|--|--|
| empirical formula   | C <sub>14</sub> H <sub>20</sub> La <sub>2</sub> N <sub>4</sub> O <sub>20</sub> | C <sub>14</sub> H <sub>20</sub> Ce <sub>2</sub> N <sub>4</sub> O <sub>20</sub> | C <sub>14</sub> H <sub>20</sub> N <sub>4</sub> O <sub>20</sub> Pr <sub>2</sub> | C <sub>14</sub> H <sub>20</sub> Nd <sub>2</sub> N <sub>4</sub> O <sub>20</sub> | C <sub>14</sub> H <sub>20</sub> N <sub>4</sub> O <sub>20</sub> Sm <sub>2</sub> |
| fw                  | 842.14   | 844.56   | 846.14   | 852.8  | 865.04   |
| cryst syst          | orthorhombic   | orthorhombic   | orthorhombic   | orthorhombic   | orthorhombic   |
| space group         | Pna <sub>2</sub> <sub>1</sub>  |
| a (Å)               | 12.1350(5)   | 12.0560(3)   | 12.0020(2)   | 11.9460(2)   | 11.8680(2)   |
| b (Å)               | 11.0417(4)   | 11.0360(3)   | 11.0080(1)   | 10.9890(2)   | 10.9620(3)   |
| c (Å)               | 19.6509(8)   | 19.5610(5)   | 19.4730(4)   | 19.4020(3)   | 19.3070(4)   |
| V (Å <sup>3</sup> ) | 2633.04(18)  | 2602.59(12)  | 2572.73(7)   | 2546.99(7)   | 2511.78(10)  |
| GOF                 | 1.078  | 0.950  | 1.044  | 1.032  | 0.858  |
| R <sub>int</sub>    | 0.0347   | 0.0534   | 0.0439   | 0.0390   | 0.0432   |
| final R indices     |  |  |  |  |  |
| [I > 2σ(I)] R1/wR2  | 0.0462/0.1139  | 0.0355/0.0755  | 0.0340/0.0822  | 0.0271/0.0643  | 0.0312/0.0582  |
| all data R1/wR2     | 0.0540/0.1159  | 0.0468/0.0771  | 0.0434/0.0836  | 0.0329/0.0658  | 0.0444/0.0595  |

effects, as will be detailed below. However, all compounds share a common structural feature, based on the always present double-

chelation mode established by the pmdc<sup>7a,18</sup> and ox ligands.<sup>19</sup> In this sense, the crystal structures **1-Ln** and **2-Ln** present metal

Table 5. Crystallographic Data and Structure Refinement Details of Compounds of 4-Eu–4-Dy and 5-La

|                                     | 4-Eu   | 4-Gd   | 4-Tb   | 4-Dy   | 5-La  |
|-------------------------------------|--|--|--|--|---|
| empirical formula                   | C <sub>14</sub> H <sub>20</sub> Eu <sub>2</sub> N <sub>4</sub> O <sub>20</sub> | C <sub>14</sub> H <sub>20</sub> Gd <sub>2</sub> N <sub>4</sub> O <sub>20</sub> | C <sub>14</sub> H <sub>20</sub> N <sub>4</sub> O <sub>20</sub> Tb <sub>2</sub> | C <sub>14</sub> H <sub>20</sub> Dy <sub>2</sub> N <sub>4</sub> O <sub>20</sub> | C <sub>7</sub> H <sub>8</sub> LaN <sub>2</sub> O <sub>9</sub> |
| fw                                  | 868.25   | 878.82   | 882.17   | 889.32   | 403.05  |
| cryst syst                          | orthorhombic   | orthorhombic   | orthorhombic   | orthorhombic   | monoclinic  |
| space group                         | Pna <sub>2</sub> <sub>1</sub>  | Pna <sub>2</sub> <sub>1</sub>  | Pna <sub>2</sub> <sub>1</sub>  | Pna <sub>2</sub> <sub>1</sub>  | P2 <sub>1</sub> /n  |
| <i>a</i> (Å)                        | 11.8280(3)   | 11.7927(4)   | 11.786(2)  | 11.760(1)  | 6.9220(11)  |
| <i>b</i> (Å)                        | 10.9430(17)  | 10.9340(3)   | 10.956(2)  | 10.938(1)  | 16.9702(2)  |
| <i>c</i> (Å)                        | 19.2610(4)   | 19.2152(7)   | 19.206(3)  | 19.167(2)  | 9.8262(2)   |
| β (deg)                             |  |  |  |  | 100.154(2)  |
| <i>V</i> (Å <sup>3</sup> )          | 2493.0(4)  | 2477.63(14)  | 2479.87(3)   | 2465.5(2)  | 1136.18(18)   |
| GOF                                 | 0.917  | 0.852  |  |  | 0.961   |
| R <sub>int</sub>                    | 0.0438   | 0.0427   |  |  | 0.0322  |
| Chi <sup>2</sup>                    |  |  | 1.51   | 1.69   |   |
| final <i>R</i> indices              |  |  |  |  |   |
| [ <i>I</i> > 2σ( <i>I</i> )] R1/wR2 | 0.0301/0.0608  | 0.0302/0.0543  |  |  | 0.0202/0.0463   |
| all data R1/wR2                     | 0.0394/0.0619  | 0.0412/0.0554  |  |  | 0.0251/0.0470   |

centers bridged by two bis-chelating pmdc ligands (mode a) and one bis-bidentate ox ligand, providing a distorted 2D honeycomb network in which the remaining coordination positions of the lanthanides are occupied by water molecules. The networks of compounds **3-Ln**, **4-Ln**, and **5-Ln** are comprised of the same topological honeycomb sheets, but some of nonchelating carboxylate oxygen atoms of pmdc ligands displace some coordinated water molecules connecting in this way (coordination modes b and c) adjacent sheets to provide overall 3D networks.

**Crystal Structure of {[Ln(μ-pmdc)(μ-ox)<sub>0.5</sub>(H<sub>2</sub>O)<sub>2</sub>]·3H<sub>2</sub>O}<sub>n</sub> [Ln = Er (1-Er), Tm (1-Tm), and Yb (1-Yb)].** The crystal building of these compounds consists of stacked [Ln(μ-pmdc)(μ-ox)<sub>0.5</sub>(H<sub>2</sub>O)<sub>2</sub>] layers separated by crystallization water molecules. The metal centers are surrounded by a N<sub>2</sub>O<sub>4</sub>Ow<sub>2</sub> donor set (Figure 2), leading to a coordination geometry close to a triangular dodecahedron (TDD) as revealed by the continuous shape measurements (CSHM) carried out by the program SHAPE [*S*(tdd) = 0.96–0.99].<sup>20</sup> The coordination Ln–N and Ln–O bond lengths and angles are within the range observed for analogous carboxylic azine ligands.<sup>21</sup>

The metal centers are joined by planar bis-bidentate pmdc ligands (Ln···Ln ca. 6.9 Å), generating corrugated Ln–pmdc chains that run along the crystallographic *b* axis with a Ln···Ln···Ln angle of 140.7–140.9°. Each chain is joined to two neighboring chains by means of the ox anion, leading to a Shubnikov hexagonal plane net parallel to the (1 0 –1) plane. The Ln···Ln distance across the bridging ox ligands is ca. 6.1 Å. The two bridging pmdc ligands are almost parallel (4.8–4.9°), but the ox ligand is nearly perpendicular to the pmdc ligands (ca. 80°). The two coordinated water molecules occupy adjacent positions in the coordination sphere of the lanthanide. The topological analysis performed by the TOPOS program package<sup>22</sup> indicates a uninodal two-dimensional hcb topological network (3-c net), the point symbol being (6<sup>3</sup>) (Figure 3).

The sheets are piled up along the *c* axis, creating distorted hexagonal channels by means of an extensive hydrogen-bonding scheme involving direct hydrogen-bonding interactions (O1w–H11···O182) between the sheets and through crystallization water molecules. The available space within the channels represents 415 Å<sup>3</sup> per unit cell (16.3%), and it is filled by

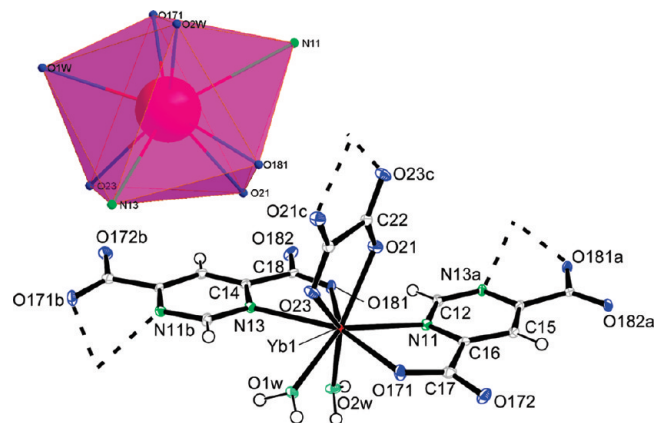


Figure 2. Coordination environment in compound 1-Yb.

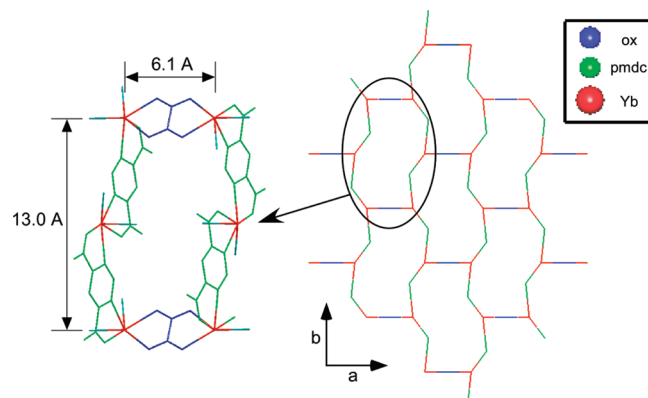
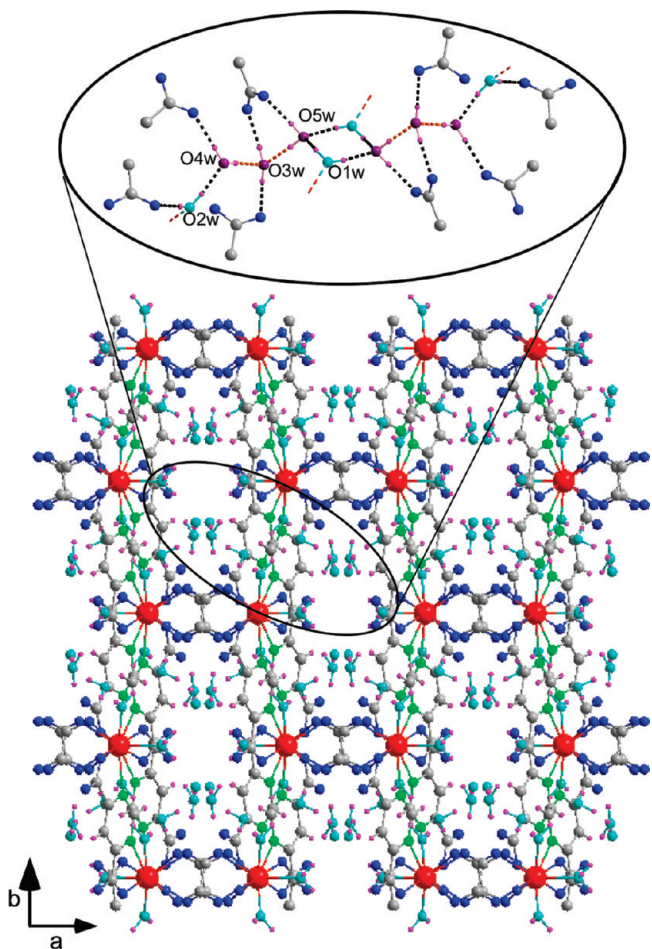


Figure 3. Simplified 2D net with hcb topology of compound 1-Yb.

hydrogen-bonded D3 discrete chains of crystallization water molecules,<sup>23</sup> which are also anchored to the walls of the channels through additional hydrogen-bonding interactions with both carboxylate oxygen atoms and coordinated water molecules (Figure 4).



**Figure 4.** Crystal building of compound **1-Yb** showing the hydrogen-bonded water clusters.

Thermal studies of compound **1-Yb** reveal that during the release of the crystallization water molecules two consecutive phase changes take place at 50 and 90 °C. (Supporting Information) The XRPD profiles of these new crystalline phases do not correspond to any of the crystal structures reported herein. Above 110 °C, a marked decrease in the crystallinity was observed during release of the coordinated water molecules, leading to an amorphous anhydrous product that remains stable from 170 to 350 °C, after which it suffers several decomposition processes to lead to  $\text{Yb}_2\text{O}_3$  as the final residue above 650 °C.

**Crystal Structure of  $\{[\text{Ln}(\mu\text{-pmdc})(\mu\text{-ox})_{0.5}(\text{H}_2\text{O})_3]\cdot 2\text{H}_2\text{O}\}_n$**  [ $\text{Ln} = \text{Dy}$  (2-Dy) and  $\text{Er}$  (2-Er)]. The crystal building of these compounds is closely related to that of the compounds **1-Ln**, although the metal centers incorporate a third coordinated water molecule, leading to a nine-coordinated  $\text{N}_2\text{O}_4\text{Ow}_3$  environment containing three chelate rings from two symmetrically related pmdc ligands and a centrosymmetric ox ligand. The shape measurements indicate that the coordination polyhedra is intermediate between the Johnson gyroelongated square pyramid (JGSP) and the triaugmented trigonal prism (TTP) [ $S(\text{jgsp}) = 1.25 - 1.35$  and  $S(\text{tpp}) = 1.65 - 1.68$ ]. A view of the coordination sphere of the metal center and an ORTEP diagram of its connectivity for compounds **2-Ln** is shown in Figure 5.

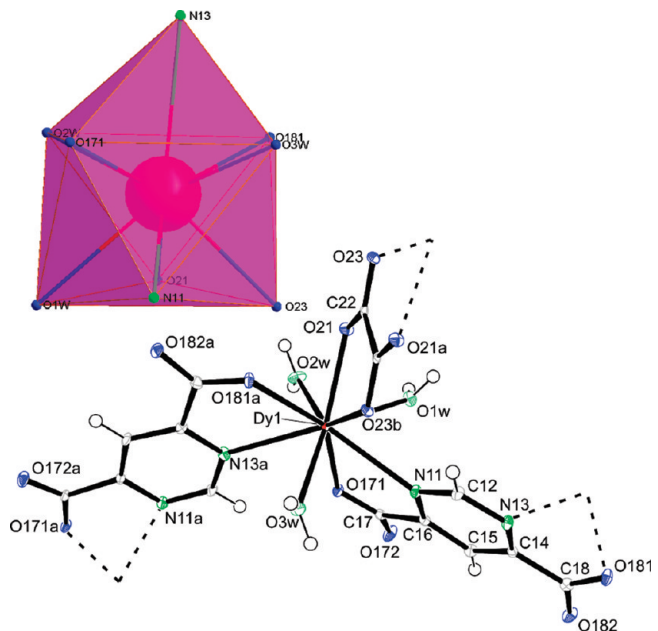


**Figure 5.** Coordination polyhedron for compound 2-Dy.

The new coordination geometry breaks the parallel disposition of the bridging pmdc ligands (dihedral angle 32.5–32.7°) and imposes more acute  $\text{Ln}\cdots\text{Ln}\cdots\text{Ln}$  angles: ca. 128° through the pmdc bridge. The ox anions, like in compounds **1-Ln**, connect the pmdc-bridged chains to generate again a two-dimensional hcb topological network (see Figure 6). The  $\text{Ln}\cdots\text{Ln}$  distances through the pmdc and ox ligands are 7.22–7.24 and 6.09–6.14 Å, respectively. In contrast to compounds **1-Ln**, substantially different dihedral angles are found between the ox ligand and the two pmdc ligands coordinated to the same metal center: 58.6° and 81.1–81.6°, respectively. Another significant difference is the relative orientation of the pmdc ligands with respect to the sheet mean plane. For compounds **1-Ln** it is nearly perpendicular to the sheet main plane, but for compounds **2-Ln** it is twisted 33.9–34.1°, in such a way that occludes the voids found in compounds **1-Ln**. In fact, the available free space in compound **2-Ln** after removal of the crystallization water molecules is smaller than that found for compounds **1-Ln** (8.4% vs 16.3%).<sup>24</sup>

The layers are packed to form a 3D supramolecular structure by an extensive hydrogen-bonding scheme. Like in compounds **1-Ln**, there are some direct hydrogen-bonding interactions ( $O1w-H11w\cdots O182$ ) that provide certain rigidity to the 3D architecture. On the other hand, the remaining coordinated  $O2w$  and  $O3w$  are hydrogen bonded to the noncoordinating oxygen atoms of the pmdc ligands belonging to the same sheet ( $O2w-H21w\cdots O172$  and  $O3w-H31w\cdots O182$ ) and stabilize in this way the relative disposition of the pmdc ligands within the sheet. The crystallization  $O4w$  and  $O5w$  water molecules are placed at the interlamellar region, establishing strong hydrogen-bonding interactions with the layer network to afford discrete tetrameric chains of the type D4, the most common pattern reported by water molecule clusters<sup>23</sup> (Figure 7).

**Crystal Structure of  $\left[\text{Ln}(\mu_3\text{-pmdc})(\mu\text{-ox})_{0.5}(\text{H}_2\text{O})_2\right] \cdot \sim 2.33\text{H}_2\text{O}\right]_n$**  [Ln = La (3-La), Ce (3-Ce), Pr (3-Pr), Nd (3-Nd), Sm (3-Sm), Eu (3-Eu), Gd (3-Gd), Tb (3-Tb), Dy (3-Dy), Ho (3-Ho), and Er (3-Er)]. 3-Ln compounds crystallize in the monoclinic  $P2_1/n$  space group at room temperature, but they

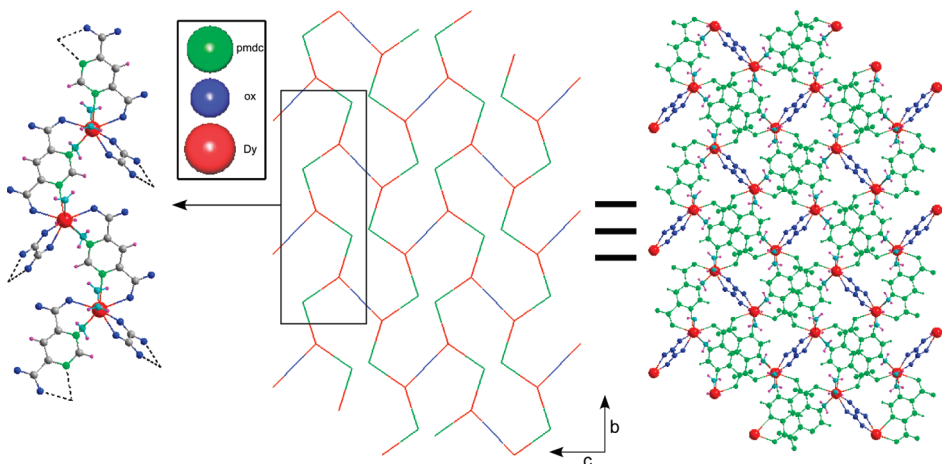


Figure 6. Two-dimensional network of compound 2-Dy.

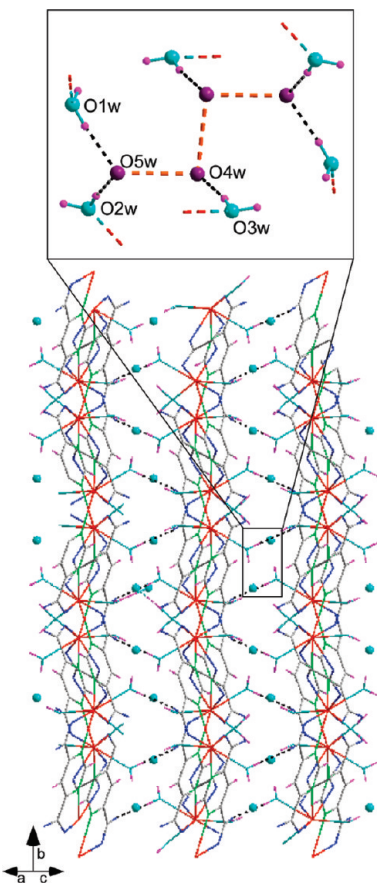


Figure 7. Three-dimensional packing of compound 2-Dy.

undergo a phase transition toward a modulated commensurate structure in the superspace group  $P2_1/n(\alpha 0\gamma)0s$  with a commensurate  $\mathbf{q}$  vector ( $\mathbf{q} = 0\ 0\ 1/3$ ) upon cooling to 100 K. The crystal structure consists of a 3D neutral open framework built up from the junction of  $\text{Ln(III)}-\text{pmdc}-\text{ox}$  layers where one of the coordinated water molecules found in compounds 2-Ln has been replaced by a previously noncoordinated pmdc oxygen atom from an adjacent sheet to give a  $\text{N}_2\text{O}_5\text{Ow}_2$  donor set around the  $\text{Ln(III)}$  centers (Figure 8). This replacement severely increases the distortion of the coordination polyhedra with regard to the

ideal shapes (JGSP and TTP), as indicated by the CShM [ $S(jgsp) = 1.98-2.18$  and  $S(ttp) = 2.94-3.07$  on going from 3-Sm to 3-Er].

The coordination of the third pmdc ligand disposes the two adjacent chelating pmdc ligands at dihedral angles of  $75.2-78.0^\circ$  maintaining the corrugation of the  $\text{Ln}\cdots\text{Ln}\cdots\text{Ln}$  angles  $139.6-140.7^\circ$ . The ox anions, like in compounds 2-Ln, arise from the chain with substantially different dihedral angles with the two pmdc ligands  $69.8-70.8^\circ$  and  $86.0-87.8^\circ$ , respectively, which hardly modifies the 2D grid. The tridentate  $\mu_3\kappa N,O:\kappa N',O':\kappa O''$ -pmdc ligand serves as a junction between layers by adopting the coordination mode **b** (Scheme 1) to lead to a 3D open framework that possesses channels along the crystallographic  $a$  axis that are filled by solvent water molecules (Figure 9). The available space within these channels of approximate dimensions of  $5 \times 7 \text{ \AA}$  represents 20.1% of the unit cell volume, and topological analysis indicates a ins-like 3D network (3,4-c net), the point symbol being  $(6^3)(6^5.8)$ .

Analysis of the superspace density map obtained by charge flipping revealed that one of the crystallization water molecules, the  $\text{O}5w$  atom, showed a discontinuity in the modulation function. Such discontinuity was modeled by shifting the basic position of the  $\text{O}5w$  atom at the  $n$  mirror plane and describing its modulation by a crenel function of width 0.5.<sup>25</sup> As a consequence, the  $\text{O}5w$  atom exists only in certain regions of the whole interval of  $x_4$  (see Supporting Information).

In order to better understand the commensurate modulation present in compounds 3-Ln, there have been represented the three basic unit cells of room temperature structure piled up along the  $c$  axis that comprise the supercell (Figure 10). The main difference between both structures is the presence or absence of the  $\text{O}5w$  crystallization water molecules along contiguous channels, involving distortions that also imply slight modifications in the coordination environment of the metal centers.

The thermogravimetric analysis performed over compound 3-Gd shows a first endothermic process that starts at  $50^\circ\text{C}$ , and it is completed around  $125^\circ\text{C}$  and corresponds to release of 2.33 water molecules (DTA peak,  $100^\circ\text{C}$ ; weight loss, exp, 9.8%, calcd, 9.4%), which is roughly the content of crystallization water molecules. The obtained product (3'-Gd) is crystalline (see Supporting Information), and indexation of its diffraction pattern gives rise to the following monoclinic unit cell parameters:  $a = 23.364(4) \text{ \AA}$ ,  $b = 10.998(2) \text{ \AA}$ ,  $c = 14.061(2) \text{ \AA}$ ,  $\beta = 103.136(9)^\circ$ , which are related to those of the supercell structure. The XRPD

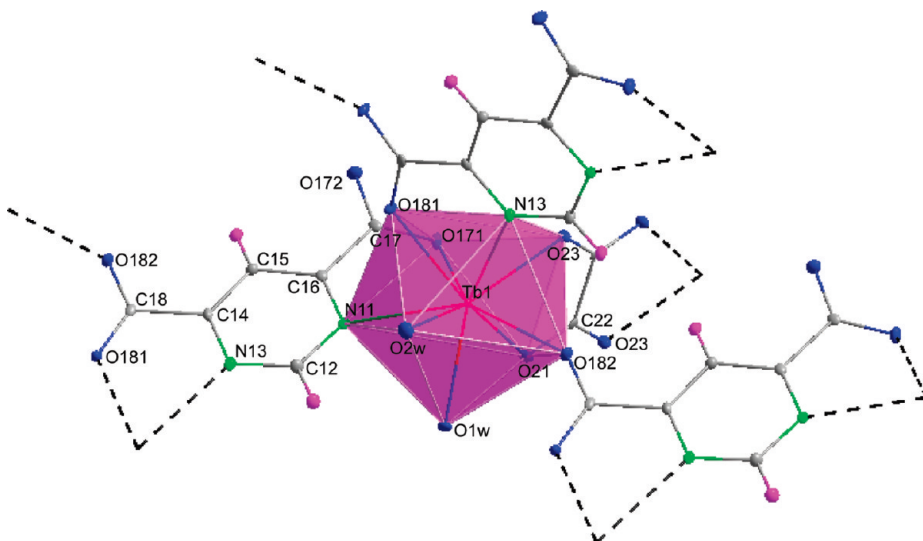


Figure 8. Fragment of compound 3-Tb showing the environment around the metal center.

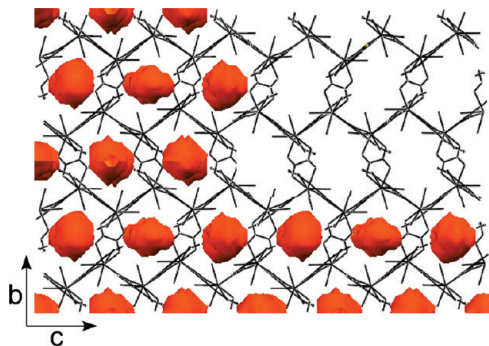


Figure 9. Packing of compound 3-Tb showing the channels (orange solid) along the [100] direction.

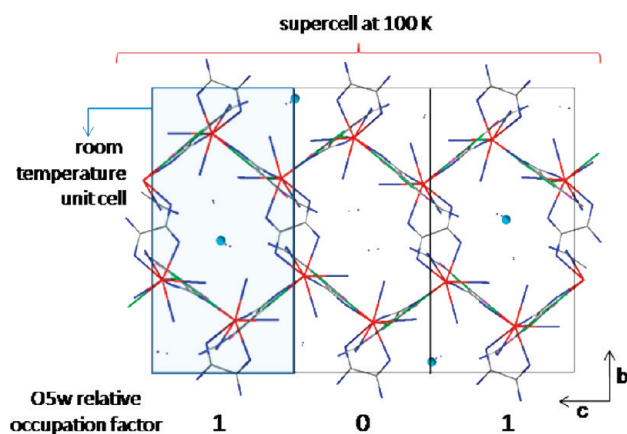
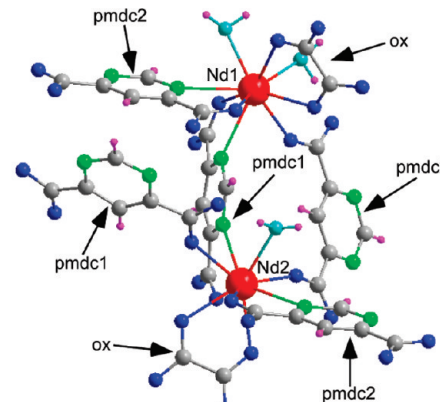


Figure 10. View of the supercell along the  $a$  axis showing the occupation factor of the O5w water molecule (light blue spheres).

patterns remain unaltered up to 210 °C, after which a decrease in the crystallinity was observed, leading to an amorphous phase that above 650 °C gives crystalline Gd<sub>2</sub>O<sub>3</sub> as the final product.

**Crystal Structure of  $\{[\text{Ln}_2(\mu_3\text{-pmdc})(\mu_4\text{-pmdc})(\mu\text{-ox})\text{-}(\text{H}_2\text{O})_3]\cdot 5\text{H}_2\text{O}\}_n$**  [ $\text{Ln} = \text{La}$  (4-La), Ce (4-Ce), Pr (4-Pr), Nd

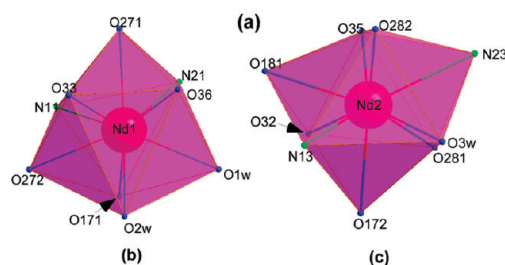
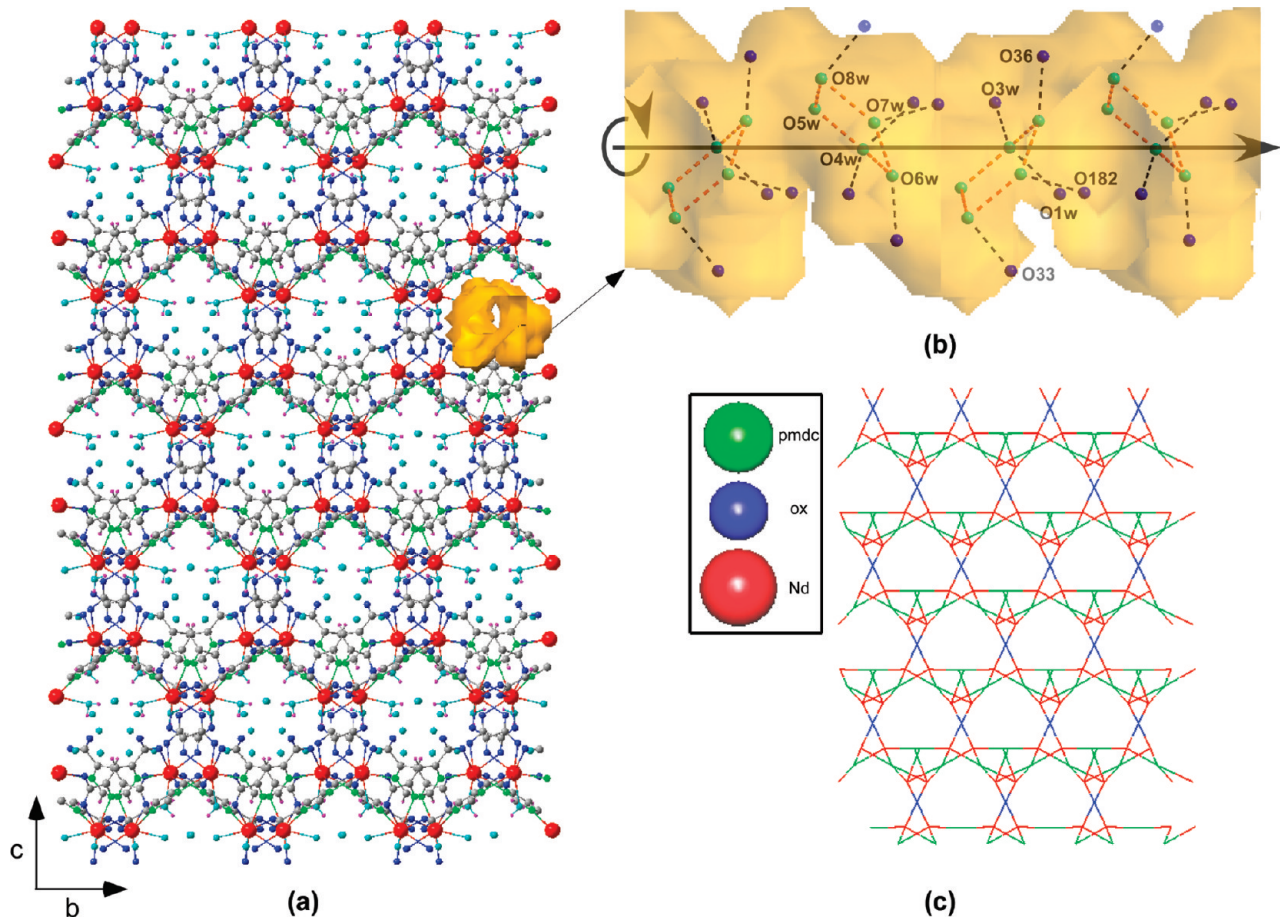


Figure 11. (a) Fragment of the crystal structure of compound 4-Nd. Coordination polyhedra of (b) Nd1 and (c) Nd2 atoms showing the numbering scheme.

(4-Nd), Sm (4-Sm), Eu (4-Eu), Gd (4-Gd), Tb (4-Tb), and Dy (4-Dy)]. Compounds 4-Ln crystallize in the acentric  $Pna2_1$  space group and contain pmdc linkers with two different coordination modes (pmdc1 adopts mode b and pmdc2 mode c). These compounds also exhibit the same 3D neutral open framework described for compounds 3-Ln, but one of the two crystallographic independent metal centers (Ln2) has a second water molecule replaced by a noncoordinated pmdc oxygen atom (Figure 11), increasing in this way the connectivity among the Ln-pmdc-ox sheets. CShM's analyses show that the  $\text{N}_2\text{O}_5\text{Ow}_2$  coordination polyhedra of Ln1 are more distorted than the



**Figure 12.** (a) Crystal packing showing the channels in compound 4-Nd. (b) Disposition of pentagonal ring clusters along the channel. (c) Schematic representation of the 3D net.

$\text{N}_2\text{O}_6\text{Ow}$  environment of Ln2 [ $S_{\text{Ln}1/\text{Ln}2}(\text{jgsp}) = 2.47-2.85/0.99-1.28$  and  $S_{\text{Ln}1/\text{Ln}2}(\text{tpp}) = 3.97-4.28/2.67-2.96$ ].

It is noteworthy that the chelating pmdc2 ligand imposes a significantly longer distance along Ln1 ··· Ln2 (7.349–7.429 Å) than the pmdc1 ligand (7.039–7.111 Å), probably due to its greater denticity that weakens the strength of the chelation. Furthermore, the pmdc1 and pmdc2 ligands are forced to be arranged almost perpendicularly, folding even further the Ln–pmdc chain (Ln ··· Ln ··· Ln 98.82–98.98°) in order to dispose outward the nonchelating carboxylate oxygen atoms of the pmdc ligands, which facilitates their coordination to the metal centers of adjacent layers.

Topological analysis of the crystal structure revealed that the structure consists of a four-nodal 3D network [(3-c)(4-c)(4-c)-(5-c)], with a point symbol of  $(4.6^2)(4.6^4.8)_2(4.6^6.8^3)$ , which is a nonpreviously registered topology in the TOPOS<sup>22</sup> database, which has been named as **jcr1** (Figure 12). This crystal structure contains noninterconnected helical  $2_1$  channels that are propagated along the  $a$  axis (free volume of  $622.6 \text{ \AA}^3$ , 24.4% per unit cell), and they are filled by hydrogen-bonded R5 pentagonal rings of solvation water molecules.<sup>23</sup>

Thermal analysis of compound 4-Ce shows the loss of four water molecules per metal between room temperature and 200 °C (exp, 18.1%; calcd, 17.1%). The anhydrous compound corresponds to a new phase of low crystallinity and remains stable up to 310 °C, after which several exothermic decomposition processes take place to give CeO<sub>2</sub> as the final product above 400 °C.

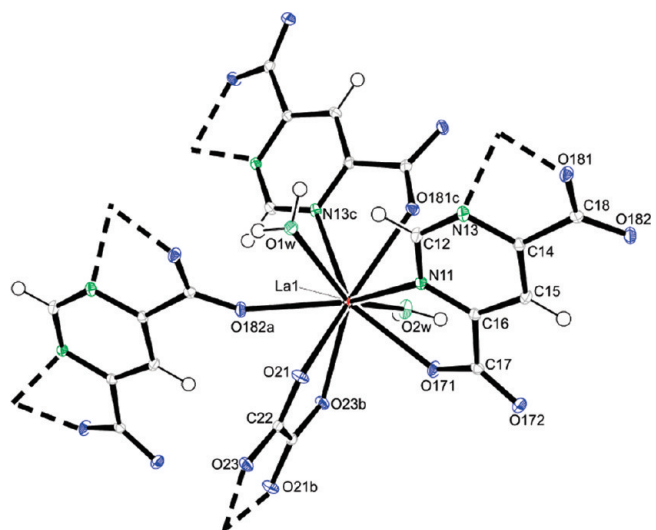


**Figure 13.** ORTEP drawing of compound **5-La** with atomic-numbering scheme.

**Crystal Structure of  $\{[\text{Ln}(\mu_3\text{-pmdc})(\mu\text{-ox})_{0.5}(\text{H}_2\text{O})_2]\cdot\text{H}_2\text{O}\}_n$**  ( $\text{Ln} = \text{La}$  (5-La) and  $\text{Ce}$  (5-Ce)). The crystal structure of compounds 5-Ln also consists of a 3D framework, with a **ins** topology, built up from the junction of the **hcb** honeycomb plane nets, but the content of crystallization water molecules is lower

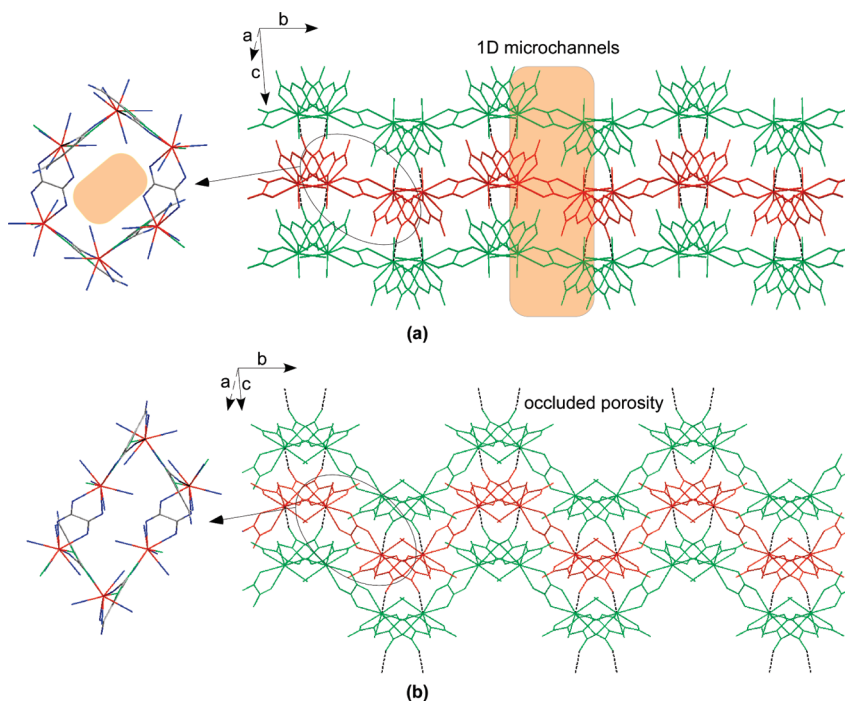
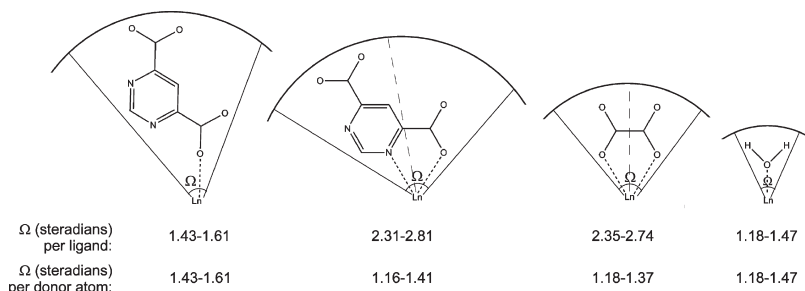


Figure 14. Comparative packing of compounds (a) 3-Nd and (b) 5-La showing the hexagonal cavities in the left side.

**Scheme 2. Solid Angle ( $\Omega$ ) Occupied by Each Ligand around the Metal Center**



than that found in compounds 3-Ln. Additionally, water molecules of the  $\text{N}_2\text{O}_5\text{Ow}_2$  donor set are placed at nonadjacent positions ( $\text{O}1\text{w}-\text{Ln}1-\text{O}2\text{w}$   $143.73^\circ$  for 5-La), in contrast to what happens for 3-Ln ( $\text{O}1\text{w}-\text{Ln}1-\text{O}2\text{w}$   $72.74-73.08^\circ$ ) (Figure 13). This stabilizes the JGSP against the TTP geometry, as can be deduced from the CShM's [ $S(jgsp) = 1.64$  and  $S(ttp) = 3.01$ ]. This arrangement forces the dihedral angle between adjacent chelating pmdc ligands to adopt a significantly lower value,  $57.8^\circ$  for 5-La and  $75.2-78.03^\circ$  for 3-Ln, but preserves the orientation of the ox ligand (dihedral angles with respect to the chelating pmdc mean planes  $67.0$  and  $77.0^\circ$ , respectively). As a consequence, the 2D sheets are no longer planar involving a remarkable dihedral angle between the mean planes of the hexagonal cavities ( $34.9^\circ$  for 5-La vs ca.  $1^\circ$  for 3-Ln) that are significantly narrower. On the other hand, the piling up of the sheets through the nonchelating  $\text{O}_{\text{COO}}^-$  atom of the pmdc ligand precludes the presence of channels similar to those found in 3-Ln and gives rise to a more compact crystal structure (Figure 14).

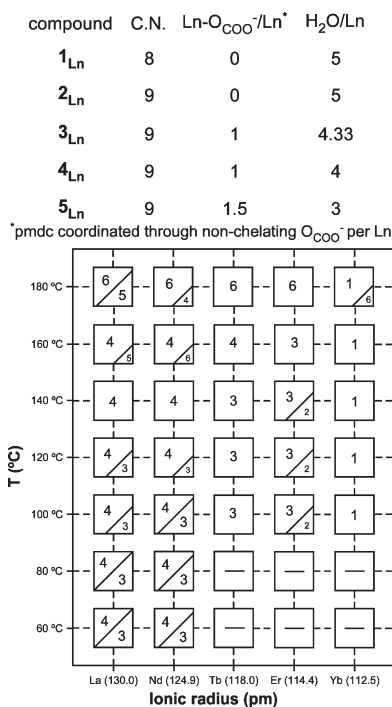
**Comments on the Ln(III)/pmdc/ox System Diversity.** The structural differences found in this system can be rationalized on the basis of two distinct factors that direct the building up of the

structures. First, the well-known entropy-driven desolvation pathway<sup>26</sup> favors release of solvent molecules and, as a consequence, generation of crystal structures with a higher connectivity among the metal nodes. On the other hand, the resulting crystal structure must pay the energetic penalty caused by the combined effect of the ligands steric hindrance and the ionic radius of the lanthanide.<sup>27</sup> In this sense, study of the ligands steric hindrance by means of the Solid-G program<sup>28</sup> revealed that the greater hindrance per occupied coordination position is due to the pmdc ligand coordinated by its nonchelating oxygen atom (Scheme 2).

In order to get deeper insight into the influence of the reaction temperature and the ionic radii of the lanthanides on the structural variety, we carried out a systematic variable-temperature study at hydrothermal conditions for five specific lanthanides. In this study,  $\text{LnX}_3$  ( $\text{X} = \text{NO}_3$  or  $\text{Cl}$ ), pyrimidine-4,6-dicarboxylic acid, and water in a molar ratio 1:2:18518 were placed in a Teflon-lined stainless steel autoclave and heated at temperatures in the range of  $60-180^\circ\text{C}$  for 3 days, after which a slow cooling ramp of  $2^\circ\text{C}/\text{h}$  was applied (Scheme 3).

As shown in Scheme 3, this study highlights the close relationship that exists between the aforementioned factors. For starters,

**Scheme 3. Structural Characteristics and Plot of Temperature vs Ionic Radius of Ln(III)–pmdc–ox Compounds**



as the ionic radius increases the coordination number of the lanthanide increases from 8 to 9 on going from the ytterbium (**1-Ln**) to erbium (**2-Ln**), avoiding the presence of the sterically more unfavorable pmdc ligand bridged by its nonchelating oxygen atom until the ionic radius is able to assume it, leading to 3D crystal structures (**3-Ln** and **4-Ln**). A similar trend is also observed with increasing temperature, so the entropic effect stabilizes denser crystal structures where the H<sub>2</sub>O/Ln ratio experiences a progressive decrease as the coordinated water molecules are replaced by nonchelating O<sub>COO</sub><sup>-</sup> atoms, reaching more compact frameworks with a lower content of crystallization molecules. As an example, it is indicative of the case of the La, where the H<sub>2</sub>O/Ln ratio decreases as the structure changes as follows **3-La** → **4-La** → **5-La**. In any case, as we have seen for the synthesis of **5-Ln** compounds and as has been suggested by other authors<sup>29</sup> factors such as the reaction time, the heating and cooling ramps could also play a relevant role. Furthermore, the continuous shape measurements have revealed that the coordination environments get closer to the ideal geometries with

decreasing ionic radius of the lanthanide. It could be attributed to a more acute energy penalty for deviations from the regular geometries as the donor atoms get closer to the metal center.

Finally, a new phase **6-Ln** has been obtained for all the metal salts by heating the solutions at 180 °C. Elemental analyses and thermogravimetric measurements suggest that compounds **6-Ln** correspond to empirical formula [Ln(pmdc)<sub>1.5</sub>(H<sub>2</sub>O)<sub>2.5</sub>].

**Magnetic Properties.** The temperature-dependent magnetic susceptibility data of compounds **1-Ln**, **3-Ln**, **4-Ln**, and **5-Ln** with the exception of those of lanthanum have been measured for polycrystalline samples.

The  $\chi_M T$  values at room temperature are close to those expected for the ground states derived from their strong spin–orbit coupling in the case of Ln<sup>III</sup> = Ce, Pr, Nd, Tb, Dy, Ho, Er, Tm, and Yb. Lowering the temperature caused a decrease in  $\chi_M T$ , which could arise from a selective depopulation of the excited Stark levels and antiferromagnetic interaction between lanthanide ions. To our knowledge, there is no available expression to determine the magnetic susceptibilities of such 2D or 3D systems with large anisotropy. To obtain a rough quantitative estimation of the magnetic interaction, these ions may be assumed to exhibit a splitting of the m<sub>j</sub> energy levels ( $H = \Delta Jz^2$ ) in an axial crystal field.<sup>30</sup> Thus,  $\chi_M(\text{Pr})$  can be described as eq 1.

$$\chi_{\text{Pr}} = \frac{Ng^2\beta^2}{kT} \frac{2e^{-\Delta/kT} + 8e^{-4\Delta/kT} + 18e^{-9\Delta/kT} + 32e^{-16\Delta/kT}}{1 + 2e^{-\Delta/kT} + 2e^{-4\Delta/kT} + 2e^{-9\Delta/kT} + 2e^{-16\Delta/kT}} \quad (1)$$

In this expression,  $\Delta$  is the zero-field splitting parameter and the Zeeman splitting was treated isotropically for the sake of simplicity. Inclusion of a  $zJ$  parameter based on the molecular field approximation<sup>30e</sup> to account for the magnetic interaction between the Ln(III) ions did not improve the fitting, and the obtained values were negligible. The  $\chi_M$  expressions for other metals have been included as Supporting Information. The best fitting results for the 50–300 K temperature range are gathered in Table 6.

Unlike most of free lanthanide ions, the energy separation of Sm(III) and Eu(III) ions between the ground state and the first excited state is so small that the first excited state may be thermally populated. In particular, according to the <sup>7</sup>F<sub>0</sub> ground state of the Eu(III) ion, it should be nonmagnetic but the nonzero room-temperature experimental  $\chi_M T$  value implies that the first excited state <sup>7</sup>F<sub>1</sub> is thermally populated. Thus, both the previously mentioned ligand-field perturbation and the possible thermal population of the higher states should be evaluated. The following expressions (eqs 2 and 3) take into account the effect of the thermal population of the higher states in the magnetic susceptibility for the Sm<sup>3+</sup> and Eu<sup>3+</sup> ions, respectively<sup>31</sup>

$$\begin{aligned} \chi_{\text{Sm}} = & \frac{N\beta^2}{3kTx} \left( \frac{2.143x + 7.347 + (42.92x + 1.641)e^{-7x/2} + (283.7x - 0.6571)e^{-8x}}{3 + 4e^{-7x/2} + 5e^{-8x} + 6e^{-27x/2} + 7e^{-20x} + 8e^{-55x/2}} \right. \\ & \left. + \frac{(620.6x - 1.94)e^{-27x/2} + (1122x - 2.835)e^{-20x} + (1813x - 3.556)e^{-55x/2}}{3 + 4e^{-7x/2} + 5e^{-8x} + 6e^{-27x/2} + 7e^{-20x} + 8e^{-55x/2}} \right) \end{aligned} \quad (2)$$

$$\begin{aligned} \chi_{\text{Eu}} = & \frac{N\beta^2}{3kTx} \left( \frac{24 + (27x - 3)/2e^{-x} + (135x - 5)/2e^{-3x} + (189x - 7/2)e^{-6x}}{1 + 3e^{-x} + 5e^{-3x} + 7e^{-6x} + 9e^{-10x} + 11e^{-15x} + 13e^{-21x}} \right. \\ & \left. + \frac{(405x - 9/2)e^{-10x} + (1485x - 11)/2e^{-27x} + (2457x - 13)2e^{-21x}}{1 + 3e^{-x} + 5e^{-3x} + 7e^{-6x} + 9e^{-10x} + 11e^{-15x} + 13e^{-21x}} \right) \end{aligned} \quad (3)$$

**Table 6. Results of the Best Least-Squares Fits of the Experimental Magnetic Data**

| compound | <i>g</i> | $\Delta$ (cm <sup>-1</sup> )  |
|----------|----------|-------------------------------|
| 1-Tm     | 1.11     | 0.34                          |
| 1-Yb     | 1.09     | 3.26                          |
| 3-Ce     | 0.82     | 5.13                          |
| 3-Pr     | 0.77     | 3.32                          |
| 3-Nd     | 0.69     | 2.15                          |
| 3-Tb     | 1.46     | 0.15                          |
| 3-Dy     | 1.31     | 0.13                          |
| 3-Ho     | 1.23     | 0.26                          |
| 3-Er     | 1.26     | 0.44                          |
| 4-Ce     | 0.81     | 5.06                          |
| 4-Pr     | 0.78     | 3.43                          |
| 4-Nd     | 0.70     | 2.28                          |
| 4-Tb     | 1.47     | 0.17                          |
| 4-Dy     | 1.26     | 0.33                          |
| 5-Ce     | 0.79     | 4.83                          |
| compound | <i>g</i> | $\lambda$ (cm <sup>-1</sup> ) |
| 3-Sm     | 0.28     | 212.00                        |
| 3-Eu     | 5.00     | 383.05                        |
| 4-Sm     | 0.29     | 215.08                        |
| 4-Eu     | 5.01     | 390.15                        |
| compound | <i>g</i> | $J$ (cm <sup>-1</sup> )       |
| 3-Gd     | 2.02     | -0.01                         |
| 4-Gd     | 2.00     | -0.01                         |

where  $x = \lambda/kT$ ,  $g$  is fixed as the theoretical value of 0.289 and 5.0 respectively, and  $\lambda$  is the spin–orbit coupling parameter. The best-fitting results for the 50–300 K temperature range are gathered in Table 6.

The temperature dependence of magnetic susceptibilities for compounds **3-Gd** and **4-Gd** were also studied. The  $\chi_M T$  values observed at 300 K are 7.98 and 7.90 cm<sup>3</sup> K mol<sup>-1</sup>, respectively, which are close to the theoretically expected one (7.88 cm<sup>3</sup> K mol<sup>-1</sup>). The Gd(III) ions are exceptions among the lanthanide series because their <sup>8</sup>S<sub>7/2</sub> ground state allows one to analyze quantitatively their magnetic interactions by applying a spin-only Hamiltonian. Taking into account that previous studies have proved that the magnetic interactions that occur through the pmde ligands are almost negligible compared to those taking place through bis-bidentated ox ligands,<sup>7,32</sup> the magnetic data have been simulated assuming a 1D lanthanide–oxalate magnetic system. Consequently, the magnetic data of both compounds were analyzed in the whole temperature range (2–300 K) using the classical Heisenberg spin model for a regular antiferromagnetic chain with  $S = 7/2$  (eq 4) (the Hamiltonian being  $H = -J\sum_i S_i \cdot S_{i+1}$ ).<sup>33</sup>

$$\chi_{\text{Gd}} = \frac{Ng^2\beta^2}{3kT} \frac{S(S+1)(1+u)}{(1-u)} \quad (4)$$

In the expression,  $u = \coth[J(S+1)/kT] - kT/J(S+1)$ ,  $J$  is the exchange coupling parameter between adjacent spins through the ox ligands, and all of the other parameters have their usual meanings.

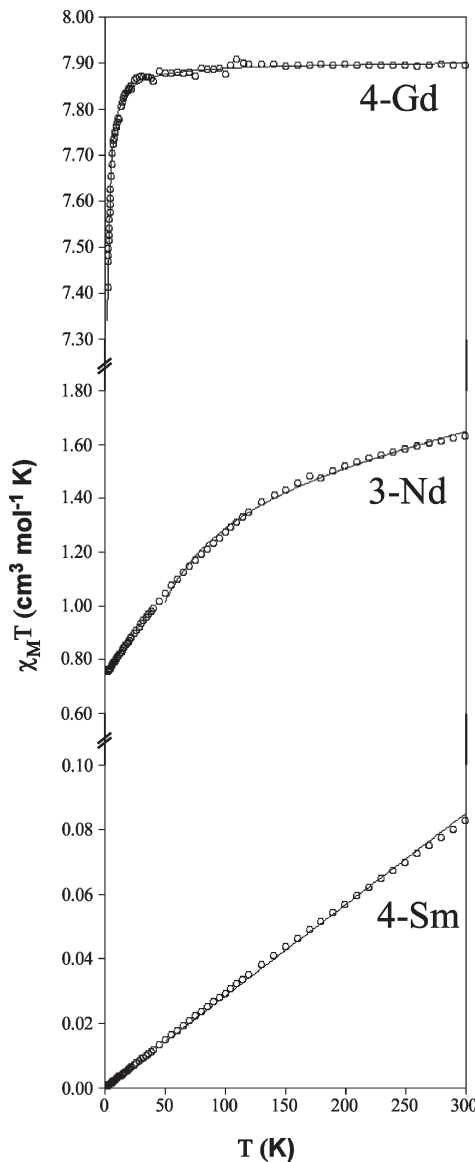


**Figure 15.**  $\chi_M T$  (○) vs  $T$  plot showing the best theoretical fit (—) for compounds **4-Gd**, **3-Nd**, and **4-Sm**.

Figure 15 shows the best-fitting curve of the  $\chi_M T$  product for three selected compounds. The results of the best least-squares fits show an almost negligible magnetic interaction among the Gd(III) ions, in good agreement with the results obtained for the other compounds of the Ln(III)/pmde/ox system and for previously published oxalate-bridged Gd(III) compounds.<sup>3k</sup> These results indicate that the magnetic behavior of these compounds, with the exception of La(III) and Gd(III), is dominated by the spin–orbit coupling and the ligand field perturbation effects. The influence of the magnetic interactions between the Ln(III) ions is almost negligible ( $|J| \leq 0.01$  cm<sup>-1</sup>).

**Luminescence Properties.** Among the newly obtained 3-Ln compounds, the europium and terbium compounds showed bright red and green luminescence under excitation at 488 nm, respectively, whereas the neodymium compound has no emission in the visible region but shows distinct emissions in the near-IR region. The luminescence spectra are typical of Eu(III), Tb(III), and Nd(III) f–f transitions, as shown in Figure 16.

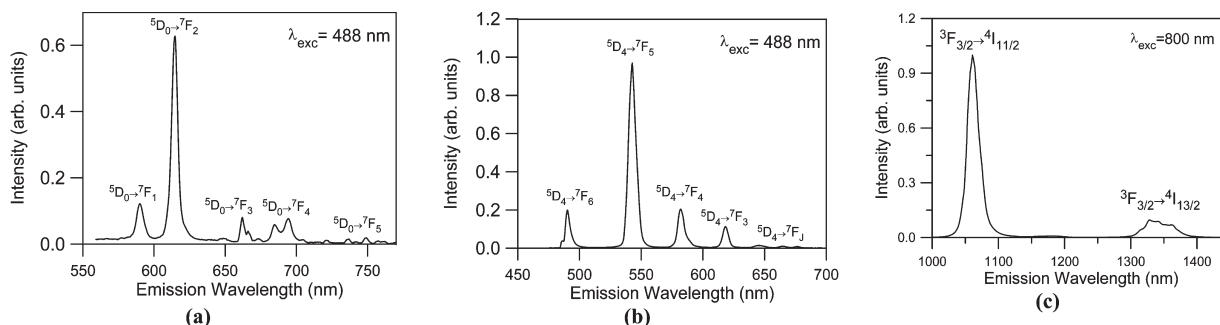


**Figure 16.** Room-temperature emission spectra obtained under excitation at 488 nm for compounds (a) 3-Eu and (b) 3-Tb and at 800 nm for (c) 3-Nd. The emissions around 650 nm in compound 3-Tb corresponds to transitions  $^5D_4 \rightarrow ^7F_J$  ( $J = 0, 1, 2$ ).

The europium-based compound (3-Eu) exhibits red luminescence with five groups of signals, which are typical for the  $\text{Eu}^{3+}$  cation.  $\text{Eu}^{3+}$  ions are excited from the ground state to  $^5D_1$  level by absorbing a 488 nm photon, and then nonradiative relaxation occurs to the  $^5D_0$  level from where five emissions located at 590, 615, 665, 690, and 750 nm take place and are assigned to  $^5D_0 \rightarrow ^7F_J$  transitions ( $J = 1, 2, 3, 4$ , and 5).<sup>34</sup> Both  $^5D_0 \rightarrow ^7F_2$  and  $^5D_0 \rightarrow ^7F_4$  transitions are mainly attributed to the electric dipole character, which is due to the nature of bonded ligands around the  $\text{Eu}^{3+}$  cation, whereas the  $^5D_0 \rightarrow ^7F_1$  one is mainly sensitive to the magnetic dipole effect created by the crystal field environment. The strongest emissions correspond to  $^5D_0 \rightarrow ^7F_2$  and  $^5D_0 \rightarrow ^7F_1$  transitions and are responsible for the brilliant-red luminescence of these complexes.<sup>35</sup> Their intensity ratio of 5:1 shows that the lanthanide atoms occupy low-symmetry sites with no inversion center in the crystal structure.

On the other hand, the terbium-based compound (3-Tb) emits a green luminescence with peaks located at 490, 540, 580, 620, and 650 nm. As expected, the intensity of the  $^5D_4 \rightarrow ^7F_5$  transition is the strongest one,<sup>36</sup> being sensitive to the nature of the atoms that form the coordination environment.

The profiles of the emission bands for compound 3-Nd are in agreement with previously reported spectra of Nd(III) complexes.<sup>37</sup> Under an 800 nm excitation in the  $^4F_{5/2}$  level, this compound displays a strong emission band at 1060.8 nm ( $^4F_{3/2} \rightarrow ^4I_{11/2}$ ) and a weaker emission band at 1328.6 nm ( $^4F_{3/2} \rightarrow ^4I_{13/2}$ ).

## CONCLUSIONS

The crystal structures of a vast family of lanthanide/pyrimidine-4,6-dicarboxylate/oxalate compounds are reported. The same bisbidentate coordination modes of the pmde and ox ligands favors their simultaneous presence in these compounds. In fact, although the *in situ* generation of the oxalate anion is due to partial decomposition of the pmde ligand during the hydrothermal process, the same compound can be obtained in higher yield by direct addition of an oxalate salt. The ion size of the Ln(III) cations and the temperature applied during synthesis are also key factors that govern the resulting crystal structure. In this way, as the ionic radius increases, the coordination number of the lanthanide increases from 8 to 9 on going from the ytterbium (**1-Ln**) to erbium (**2-Ln**), and only when the ionic radius is able to assume the presence of the sterically more hindrance  $\mu_3$ -pmde ligand, 3D architectures are obtained. A similar trend is also observed with increasing temperature, so the entropic effect stabilizes denser crystal structures where the  $\text{H}_2\text{O}/\text{Ln}$  ratio experiments a progressive decrease.

The magnetic behavior of the compounds is dominated by the spin-orbit coupling and ligand field perturbation with an almost negligible exchange coupling between the lanthanide atoms. Finally, the europium and terbium compounds show the characteristic red and green luminescence, respectively, the emission spectra being in good agreement with the crystal structure. Additionally, the neodymium compound shows emissions from the  $^4F_{3/2}$  level in the near-IR region.

## ASSOCIATED CONTENT

**S Supporting Information.** Elemental analyses, IR data, X-ray analysis, thermogravimetric measurements, magnetic susceptibility data, and cif files. This material is available free of charge via the Internet at <http://pubs.acs.org>.

## AUTHOR INFORMATION

### Corresponding Author

\*Fax: +34-94601-3500. E-mail: oscar.castillo@ehu.es.

## ACKNOWLEDGMENT

Financial support from the Ministerio de Ciencia e Innovación (Project MAT2008-05690/MAT) and the Gobierno Vasco (IT477-10) is gratefully acknowledged. We also thank the Universidad del País Vasco/Euskal Herriko Unibertsitatea for predoctoral fellowships (PIFA01/2007/021). Technical and human support provided by SGIker (UPV/EHU, MICINN, GV/EJ, ESF) is gratefully acknowledged.

## REFERENCES

- (a) Visinescu, D.; Fabelo, O.; Ruiz-Pérez, C. *CrystEngComm* **2010**, *12*, 2454–2465. (b) Eddaoudi, M.; Moler, D. B.; Li, H. L.; Chen, B. L.; Reineke, T. M.; O’Keeffe, M.; Yaghi, O. M. *Acc. Chem. Res.* **2001**, *34*, 319–330. (c) Eddaoudi, M.; Kim, J.; Rosi, N.; Vodak, D.; Wachter, J.; O’Keeffe, M.; Yaghi, O. M. *Science* **2002**, *295*, 469–472. (d) Yaghi, O. M.; O’Keeffe, M.; Ockwig, N. W.; Chae, H. K.; Eddaoudi, M.; Kim, J. *Nature* **2003**, *423*, 705–714. (e) Ockwig, N. W.; Delgado-Friedrichs, O.; O’Keeffe, M.; Yaghi, O. M. *Acc. Chem. Res.* **2005**, *38*, 176–182. (f) Kondo, M.; Okubo, T.; Asami, A.; Noro, S.; Yoshitomi, T.; Kitagawa, S.; Ishii, T.; Matsuzaka, H.; Seki, K. *Angew. Chem., Int. Ed.* **1999**, *38*, 140–143.
- (2) (a) Maji, T. K.; Mostafa, G.; Chang, H.-C.; Kitagawa, S. *Chem. Commun.* **2005**, 2436–2438. (b) Shiga, T.; Ito, N.; Hidaka, A.; Ohkawa, H.; Kitagawa, S.; Ohba, M. *Inorg. Chem.* **2007**, *46*, 3492–3501. (c) Reineke, T. M.; Eddaoudi, M.; Fehr, M.; Kelley, D.; Yaghi, O. M. *J. Am. Chem. Soc.* **1999**, *121*, 1651–1657. (d) Thirumurugan, A.; Natarajan, S. *Dalton Trans.* **2004**, 2923–2928. (e) Long, D. L.; Blake,

- A. J.; Champness, N. R.; Wilson, C.; Schröder, M. *Angew. Chem., Int. Ed.* **2001**, *40*, 2443–2447. (f) Wan, Y. H.; Jin, L. P.; Wang, K.; Zhang, L. P.; Zheng, X. J.; Lu, S. Z. *New J. Chem.* **2002**, *26*, 1590–1596. (g) Alleyne, B. D.; Williams, A. R.; Hall, L. A.; White, A. J. P.; Williams, D. J. *Inorg. Chem.* **2001**, *40*, 1045–1051. (h) Pan, L.; Zheng, N. W.; Wu, Y. G.; Nan, S.; Yang, R. Y.; Huang, X. Y.; Li, J. *Inorg. Chem.* **2001**, *40*, 828–830. (i) Sun, Y.-Q.; Zhang, J.; Yang, G.-Y. *Chem. Commun.* **2006**, 1947–1949. (j) Sun, Y.-Q.; Zhang, J.; Yang, G. Y. *Chem. Commun.* **2006**, 4700–4702. (k) Benelli, C.; Gatteschi, D. *Chem. Rev.* **2002**, *102*, 2369–2387. (l) Cañadillas-Delgado, L.; Martín, T.; Fabelo, O.; Pasán, J.; Delgado, F. S.; Lloret, F.; Julve, M.; Ruiz-Pérez, C. *Chem.—Eur. J.* **2010**, *16*, 4037–4047.
- (3) (a) Liu, W. S.; Jiao, T. Q.; Li, Y. Z.; Liu, Q. Z.; Tan, M. Y.; Wang, H.; Wang, L. F. *J. Am. Chem. Soc.* **2004**, *126*, 2280–2281. (b) Ma, B. Q.; Zhang, D. S.; Gao, S.; Jin, T. Z.; Yan, C. H.; Xu, G. X. *Angew. Chem., Int. Ed.* **2000**, *39*, 3644–3646. (c) Serre, C.; Stock, N.; Bein, T.; Férey, G. *Inorg. Chem.* **2004**, *43*, 3159–3163. (d) Mancino, G.; Ferguson, A. J.; Beeby, A.; Long, N. J.; Jones, T. S. *J. Am. Chem. Soc.* **2005**, *127*, 524–525. (e) Bunzli, J. C. G.; Piguet, C. *Chem. Rev.* **2002**, *102*, 1897–1928. (f) Tsukube, H.; Shinoda, S. *Chem. Rev.* **2002**, *102*, 2389–2403. (g) Capocchi, S.; Renault, O.; Moon, D. G.; Halim, M.; Etchells, M.; Dobson, P. J.; Salata, O. V.; Christou, V. *Adv. Mater.* **2000**, *12*, 1591–1594. (h) Kido, J.; Okamoto, Y. *Chem. Rev.* **2002**, *102*, 2357–2368. (i) Sutter, J.-P.; Dhers, S.; Rajamani, R.; Ramasesha, S.; Costes, J.-P.; Duhayon, C.; Vendier, L. *Inorg. Chem.* **2009**, *48*, 5820–5828. (j) Cañadillas-Delgado, L.; Fabelo, O.; Pasán, J.; Delgado, F. S.; Lloret, F.; Julve, M.; Ruiz-Pérez, C. *Dalton Trans.* **2010**, *39*, 7286–7293. (k) Cañadillas-Delgado, L.; Pasán, J.; Fabelo, O.; Hernández-Molina, M.; Lloret, F.; Julve, M.; Ruiz-Pérez, C. *Inorg. Chem.* **2006**, *45*, 10585–10594. (l) Baggio, R.; Calvo, R.; Garland, M. T.; Peña, O.; Perec, M.; Rizzi, A. *Inorg. Chem.* **2006**, *44*, 8979–8987.
- (4) (a) Pan, L.; Huang, X. Y.; Li, J.; Wu, Y. G.; Zheng, N. W. *Angew. Chem., Int. Ed.* **2000**, *39*, 527–530. (b) Li, X.; Shi, Q.; Sun, D. F.; Bi, W. H.; Cao, R. *Eur. J. Inorg. Chem.* **2004**, 2747–2753. (c) He, Z.; Gao, E. Q.; Wang, Z. M.; Yan, C. H.; Kurmoo, M. *Inorg. Chem.* **2005**, *44*, 862–874. (d) Yang, P.; Wu, J.-Z.; Yu, Y. *Inorg. Chim. Acta* **2009**, *362*, 1907–1912.
- (5) (a) Kiritsis, V.; Michaelides, A.; Skoulika, S.; Golhen, S.; Ouahab, L. *Inorg. Chem.* **1998**, *37*, 3407–3410. (b) Long, D. L.; Blake, A. J.; Champness, N. R.; Schröder, M. *Chem. Commun.* **2000**, 1369–1370. (c) Long, D. L.; Blake, A. J.; Champness, N. R.; Wilson, C.; Schröder, M. *J. Am. Chem. Soc.* **2001**, *123*, 3401–3402. (d) Wang, Z.; Jin, C. M.; Shao, T.; Li, Y. Z.; Zhang, K. L.; Zhang, H. T.; You, X. Z. *Inorg. Chem. Commun.* **2002**, *5*, 642–648.
- (6) (a) Serre, C.; Férey, G. *J. Mater. Chem.* **2002**, *12*, 3053–3057. (b) Serpaggi, F.; Férey, G. *J. Mater. Chem.* **1998**, *8*, 2749–2755. (c) Serpaggi, F.; Férey, G. *Inorg. Chem.* **1999**, *38*, 4741–4744. (d) Yang, A.-H.; Gao, H.-L.; Cui, J.-Z.; Zhao, B. *CrysEngComm* **2011**, *13*, 1870–1876. (e) Henry, N.; Costenoble, S.; Lagrenée, M.; Loiseau, T.; Abraham, F. *CrysEngComm* **2011**, *13*, 251–258. (f) Cai, B.; Yang, P.; Dai, J.-W.; Wu, J.-Z. *CrysEngComm* **2011**, *13*, 985–991.
- (7) (a) Beobide, G.; Wang, W. G.; Castillo, O.; Luque, A.; Román, P.; Tagliabue, G.; Galli, S.; Navarro, J. A. R. *Inorg. Chem.* **2008**, *47*, 5267–5277. (b) Beobide, G.; Castillo, O.; Luque, A.; García-Couceiro, U.; García-Terán, J. P.; Román, P. *Dalton Trans.* **2007**, 2669–2680.
- (8) Hunt, R. R.; McOmie, J. F. W.; Sayer, E. R. *J. Chem. Soc.* **1959**, 525–530.
- (9) Earnshaw, A. *Introduction to Magnetochemistry*; Academic Press: London, 1968.
- (10) Ollendorf, W.; Weigel, F. *Inorg. Nucl. Chem. Lett.* **1969**, *5*, 263–269.
- (11) *CrysAlis RED*, version 1.171.33.55; Oxford Diffraction: Wroclaw, Poland, 2010.
- (12) Altomare, A.; Cascarano, M.; Giacovazzo, C.; Guagliardi, A. *J. Appl. Crystallogr.* **1993**, *26*, 343–350.
- (13) Sheldrick, G. M. *SHELXL-97, Program for X-ray Crystal Structure Refinement*; University of Göttingen: Göttingen, Germany, 1997.
- (14) Farrugia, L. J. *J. Appl. Crystallogr.* **1999**, *32*, 837–838.
- (15) Oszlányi, G.; Sütő, A. *Acta Crystallogr., Sect. A* **2004**, *60*, 134–141.
- (16) Petricek, V.; Dusek, M.; Palatinus, L. *Jana2006. The crystallographic computing system*; Institute of Physics: Praha, Czech Republic, 2006.
- (17) (a) Rodríguez-Carvajal, J. *FULLPROF*, a Program for Rietveld Refinement and Pattern Matching Analysis. *Abstracts of the Satellite Meeting on Powder Diffraction of the XVth Congress of the IUCr*, Toulouse, France, 1990; p 127. (b) Rodríguez-Carvajal, J. *FULLPROF* 2000, version 2.5d; Laboratoire Léon Brillouin (CEA-CNRS), Centre d'Études de Saclay, Gif sur Yvette Cedex: France, 2003.
- (18) Beobide, G.; Castillo, O.; Cepeda, J.; Luque, A.; Pérez-Yáñez, S.; Román, P.; Vallejo-Sánchez, D. *Eur. J. Inorg. Chem.* **2011**, 68–77.
- (19) See for example: (a) García-Couceiro, U.; Castillo, O.; Cepeda, J.; Lanchas, M.; Luque, A.; Pérez-Yáñez, S.; Román, P.; Vallejo-Sánchez, D. *Inorg. Chem.* **2010**, *49*, 11346–11361. (b) Pérez-Yáñez, S.; Castillo, O.; Cepeda, J.; García-Terán, J. P.; Luque, A.; Román, P. *Inorg. Chim. Acta* **2011**, *365*, 211–219.
- (20) Llunell, M.; Casanova, D.; Cirera, J.; Bofill, J. M.; Alemany, P.; Alvarez, S.; Pinsky, M.; Avnir, D. *SHAPE v1.7*, University of Barcelona, Barcelona, 2010.
- (21) (a) Shi, F.-N.; Cunha-Silva, L.; Trindade, T.; Paz, F. A. A.; Rocha, J. *Cryst. Growth Des.* **2009**, *9*, 2098–2109. (b) Li, S.; Chen, Y.; He, H.-M.; Ma, Y.-F. *Acta Crystallogr., Sect. E* **2009**, *65*, m411. (c) Huang, Y.-G.; Wu, B.-L.; Yuan, D.-Q.; Xu, Y.-Q.; Jiang, F.-L.; Hong, M.-C. *Inorg. Chem.* **2007**, *46*, 1171–1176.
- (22) TOPOS Main Page. <http://www.topos.ssu.samara.ru> (accessed Nov 2010). Blatov, V. A. *IuCr Comp. Comm. Newslett.* **2006**, *7*, 4–38.
- (23) Infantes, L.; Chisholm, J.; Motherwell, S. *CrystEngComm* **2003**, *5*, 480–486.
- (24) Spek, A. L. *J. Appl. Crystallogr.* **2003**, *36*, 7–13.
- (25) Palatinus, L.; Dusek, M.; Glaum, R.; El Bali, B. *Acta Cryst., Sect. B* **2006**, *62*, 556–566.
- (26) Forster, P. M.; Burbank, A. R.; Livage, C.; Férey, G.; Cheetham, A. K. *Chem. Commun.* **2004**, 368–369.
- (27) Shannon, R. D. *Acta Crystallogr., Sect. A* **1976**, *32*, 751–767.
- (28) Guzei, I. A.; Wendt, M. *Dalton Trans.* **2006**, 3991–3999.
- (29) Mahata, P.; Prabu, M.; Natarajan, S. *Inorg. Chem.* **2008**, *47*, 8451–8463.
- (30) (a) Kawha, I. A.; Selbin, J.; O'Connor, C. J.; Foise, J. W.; McPherson, G. L. *Inorg. Chim. Acta* **1988**, *148*, 265–272. (b) Ke, H.; Zhao, L.; Xu, G.-F.; Guo, Y.-N.; Tang, J.; Zhang, X.-Y.; Zhang, H.-J. *Dalton Trans.* **2009**, 10609–10613. (c) Li, B.; Gu, W.; Zhang, L. Z.; Qu, J.; Ma, Z. P.; Liu, X.; Liao, D. Z. *Inorg. Chem.* **2006**, *45*, 10425–10427. (d) Ouyang, Y.; Zhang, W.; Xu, N.; Xu, G. F.; Liao, D. Z.; Yoshimura, K.; Yan, S. P.; Cheng, P. *Inorg. Chem.* **2007**, *46*, 8454–8456. (e) O'Connor, C. J. *Prog. Inorg. Chem.* **1982**, *29*, 203–283.
- (31) (a) Li, Y.; Zheng, F. K.; Liu, X.; Zou, W. Q.; Guo, G. C.; Lu, C. Z.; Huang, J. S. *Inorg. Chem.* **2006**, *45*, 6308–6316. (b) Andruh, M.; Bakalbassis, E.; Kahn, O.; Trombe, J. C.; Porcher, P. *Inorg. Chem.* **1993**, *32*, 1616–1622. (c) Wang, Y.; Li, X. L.; Wang, T. W.; Song, Y.; You, X. Z. *Inorg. Chem.* **2010**, *49*, 969–976. (d) Lin, S.-Y.; Zhao, L.; Xu, G.-F.; Guo, Y.-N.; Liu, G.-X.; Tang, J. *J. Chem. Crystallogr.* **2011**, *41*, 77–81.
- (32) (a) Masciocchi, N.; Galli, S.; Tagliabue, G.; Sironi, A.; Castillo, O.; Luque, A.; Beobide, G.; Wang, W. G.; Romero, M. A.; Bareja, E.; Navarro, J. A. R. *Inorg. Chem.* **2009**, *48*, 3087–3094. (b) Julve, M.; Verdaguera, M.; Kahn, O.; Gleizes, A.; Philoche-Levisalles, M. *Inorg. Chem.* **1983**, *22*, 368–370. (c) Julve, M.; Verdaguera, M.; Gleizes, A.; Philoche-Levisalles, M.; Kahn, O. *Inorg. Chem.* **1984**, *23*, 3808–3818.
- (33) (a) Cañadillas-Delgado, L.; Fabelo, O.; Pasán, J.; Delgado, F. S.; Lloret, F.; Julve, M.; Ruiz-Pérez, C. *Dalton Trans.* **2010**, 7286–7293. (b) Xu, N.; Shi, W.; Liao, D.-Z.; Yan, S.-P.; Cheng, P. *Inorg. Chem.* **2008**, *47*, 8748–8756. (c) Fisher, M. E. *Am. J. Phys.* **1964**, *32*, 343–346.
- (34) Richardson, F. S. *Chem. Rev.* **1982**, *82*, 541–552.
- (35) (a) de Bettencourt-Dias, A. *Inorg. Chem.* **2005**, *44*, 2734–2741. (b) Law, G. L.; Wong, K. L.; Zhou, X. J.; Wong, W. T.; Tanner, P. A. *Inorg. Chem.* **2005**, *44*, 4142–4144.

(36) Bünzli, J.-C. G. In *Lanthanide Probes in Life, Chemical and Earth Sciences, Theory and Practice*; Bünzli, J.-C. G., Choppin, G. R., Eds.; Elsevier: Amsterdam, 1989; Chapter 7.

(37) (a) Castro, A.; Enjalbert, R.; Lloyd, D.; Rasines, I.; Galy, J. *J. Solid State Chem.* **1990**, *85*, 100–107. (b) Nikiforov, G. B.; Kusainova, A. M.; Berdonosov, P. S.; Dolgikh, V. A.; Lightfoot, P. *J. Solid State Chem.* **1999**, *146*, 473–477. (c) Song, J. L.; Mao, J. G. *Chem.—Eur. J.* **2005**, *11*, 1417–1424.